Biomaterials 318 (2025) 123174

Contents lists available at ScienceDirect

Biomaterials

journal homepage: www.elsevier.com/locate/biomaterials

Enhancing biofabrication: Shrink-resistant collagen-hyaluronan composite hydrogel for tissue engineering and 3D bioprinting applications

Kaveh Roshanbinfar [a], Austin Donnelly Evans [b], Sumanta Samanta [b], Maria Kolesnik-Gray [c], Maren Fiedler [a], Vojislav Krstic [c,d], Felix B. Engel [a,**,*], Oommen P. Oommen [e,*,*]

[a] Experimental Renal and Cardiovascular Research, Department of Nephropathology, Institute of Pathology and Department of Cardiology, Friedrich-Alexander-Universität Erlangen-Nürnberg (FAU), 91054, Erlangen, Germany
[b] Bioengineering and Nanomedicine Group, Faculty of Medicine and Health Technologies, Tampere University, 33720, Tampere, Finland
[c] Department of Physics, Friedrich-Alexander-Universität Erlangen-Nürnberg (FAU), Staudtstr. 7, 91058, Erlangen, Germany
[d] Department of Physics, Wake-Forest-University, Winston Salem, NC, 27109, USA
[e] School of Pharmacy and Pharmaceutical Sciences, Cardiff University, King Edward VII Avenue, Cardiff, CF10 3NB, UK

ARTICLE INFO

Keywords:
Hydrogel
Cardiac
Tissue engineering
Shrinkage
Shrink-resistant
3D bioprinting

ABSTRACT

Biofabrication represents a promising technique for creating tissues for regeneration or as models for drug testing. Collagen-based hydrogels are widely used as suitable matrix owing to their biocompatibility and tunable mechanical properties. However, one major challenge is that the encapsulated cells interact with the collagen matrix causing construct shrinkage. Here, we present a hydrogel with high shape fidelity, mimicking the major components of the extracellular matrix. We engineered a composite hydrogel comprising gallic acid (GA)-functionalized hyaluronic acid (HA), collagen I, and HA-coated multiwall carbon nanotubes (MWCNT). This hydrogel supports cell encapsulation, exhibits shear-thinning properties enhancing injectability and printability, and importantly significantly mitigates shrinkage when loaded with human fibroblasts compared to collagen I hydrogels (~20 % vs. > 90 %). 3D-bioprinted rings utilizing human fibroblast-loaded inks maintain their shape over 7 days in culture. Furthermore, inclusion of HAGA into collagen I hydrogels increases mechanical stiffness, radical scavenging capability, and tissue adhesiveness. Notably, the here developed hydrogel is also suitable for human induced pluripotent stem cell-derived cardiomyocytes and allows printing of functional heart ventricles responsive to pharmacological treatment. Cardiomyocytes behave similar in the newly developed hydrogels compared to collagen I, based on survival, sarcomere appearance, and calcium handling. Collectively, we developed a novel material to overcome the challenge of post-fabrication matrix shrinkage conferring high shape fidelity.

1. Introduction

Biofabrication is a promising approach for generating tissues and organ-like structures as predictive, diagnostic, and explorative *in vitro* models as well as functional replacements for injured tissues. The goal is to generate biologically functional products with structural organization from living cells, bioactive molecules, biomaterials, cell aggregates, such as microtissues, or hybrid cell-material constructs, through 3D bioprinting or bioassembly and subsequent tissue maturation processes [1]. Biofabrication enables production from computer designs or medical images of patient-specific constructs or implants that match the geometrically complex and irregular shapes of the native tissue. Notably, the complex architecture of a tissue/organ plays a crucial role in facilitating tissue/organ function [2,3]. A significant challenge remains to engineer a cytocompatible material that not only allows optimal fabrication (e.g. shear thinning for 3D bioprinting) and provides favorable mechanical and biological properties for cells, but also a material that is resistant against cell-induced shrinkage to maintain the original biofabricated shape over long culture periods.

Collagen is one of the most abundant proteins of the extracellular

* Corresponding author. School of Pharmacy and Pharmaceutical Sciences, Cardiff University, King Edward VII Avenue, Cardiff, CF10 3NB, UK.
** Corresponding author. Experimental Renal and Cardiovascular Research, Department of Nephropathology, Institute of Pathology and Department of Cardiology, Friedrich-Alexander-Universität Erlangen-Nürnberg (FAU); 91054, Erlangen, Germany.
E-mail addresses: Felix.Engel@uk-erlangen.de (F.B. Engel), OommenO@cardiff.ac.uk (O.P. Oommen).
* authors contributed equally/shared last authors.

https://doi.org/10.1016/j.biomaterials.2025.123174
Received 12 September 2024; Received in revised form 21 January 2025; Accepted 5 February 2025
Available online 10 February 2025
0142-9612/© 2025 The Authors. Published by Elsevier Ltd. This is an open access article under the CC BY license (http://creativecommons.org/licenses/by/4.0/).

matrix (ECM) in most tissues/organs, which constitutes ~25 % of our body mass [4] and it continues to be widely used for tissue engineering and 3D cell culture [5–7]. Collagen and other ECM proteins, such as fibronectin, vitronectin, laminin, and nephronectin possess cell adhesive RGD rich domains [8–11] that play a major role in mechanotransduction [12,13]. The encapsulated cells within these ECM protein-derived matrices attach to the RGD adhesive motifs via integrins and exert traction forces through focal adhesions connected to their actin cytoskeletons [14]. In principle, as the cell density increases, the traction forces increase, resulting in an increased matrix stiffness and bulk shrinkage that influences the viability and functionality of the encapsulated cells. Notably, encapsulation of fibroblasts in collagen hydrogels also triggers contraction of the hydrogel resulting in significant apoptosis of the encapsulated cells [15].

Hydrogels derived from hyaluronic acid (HA) are also widely used for *in vitro* 3D cultures as HA is an important glycosaminoglycan present in the ECM that not only provides viscoelasticity, but also influences cell proliferation, migration, differentiation, wound healing, and immune response [16]. Cells cultured within HA hydrogels interact with the matrix via CD44 receptors, however they remain rounded and do not spread, as the HA lacks cell-adhesive motifs. Interestingly, grafting of adhesive molecules such as dopamine or gallic acid to HA-gels [17] alters this behavior as these molecules effectively trap the cell-produced ECM and remodel the matrix, imparting new properties, for example, to maintain differentiated hPSC-derived neurons [18] or induce immunosuppressive characteristics [19].

Several strategies have been devised to address the hydrogel shrinkage and stability issues. For example, cell-free hydroxyapatite ink with cell-laden alginate-methylcellulose ink was printed in a layer-by-layer fashion to fabricate bone tissues with improved stability [20]. While this approach improved the overall stability of printed constructs, the shrinkage of the cell-laden hydrogel was not investigated. Further efforts have been taken to reinforce 3D-bioprinted constructs post-fabrication by oxidized sucrose mediated crosslinking of 3D-bioprinted cardiac constructs [21] or by reinforcing the 3D-bioprinted constructs of fibroblast-laden HA-aldehyde and carboxymethylcellulose-doped gelatin-alginate hydrogels through secondary ionic crosslinking using $CaCl_2$ [22]. The post-fabrication treatment of these 3D constructs rendered greater mechanical properties. The shrinkage of cell-laden hydrogels is more prominent in protein-based gels when compared to other ECM mimetic gels. Interestingly, incorporation of HA into collagen gels would disperse the stress induced by cell attachment to the matrix and enhance the viscoelastic properties [23]. Although, shrinkage of 3D constructs is detrimental for maintaining structural fidelity and precision, controlled shrinkage of the matrix by ionic complexation of the 3D-printed construct was utilized for controlled enhancement of the resolution in printed constructs [24]. In order to improve shape fidelity of collagen-based hydrogels, bovine collagen I was modified with azide groups and crosslinked with 4-arm polyethylene glycol molecules with bicyclononyne end groups (SPAAC Collagen) [25]. These constructs containing mesenchymal stem cells showed less shrinkage compared to unmodified cell-laden collagen hydrogels. Nevertheless, extended crosslinking time of 2 h in this case can negatively affect cell viability. Thus, an alternative method with shorter crosslinking kinetics can advance the efforts in generating shrink-resistant hydrogels.

We have recently reported the formulation of hydrazone crosslinked HA-based bioink embedded with collagen for 3D bioprinting of corneal epithelium and stroma [26], wherein the collagen was mixed with HA building blocks without any chemical crosslinking. More importantly, we found that bioinks of collagen I and HA allow direct 3D bioprinting of functional cardiac ventricles utilizing human induced pluripotent stem cell (hiPSC) derived cardiomyocytes [27]. However, these ventricles consisted only of hiPSC-cardiomyocytes as the addition of fibroblasts would have compacted the ventricles to "balls" of cardiac tissue. Yet, as fibroblasts greatly improve the contractility of engineered cardiac tissues [28], we intend to design the next generation of bioinks in which HA and collagen are covalently crosslinked without using any toxic catalysts or crosslinkers. While direct crosslinking of HA-collagen hydrogels through acrylation of collagen or indirect approaches employing intermediate linkers seem useful, these techniques suffer from several drawbacks: (i) They are non-selective, cumbersome, and lack precise control over the degree of crosslinking, resulting in heterogeneous crosslinks. (ii) This heterogeneity leads to batch-to-batch variability, compromising the stability and functionality of the crosslinked materials. We have recently discovered the unique ability of GA to generate free radicals at physiological pH [17] that could be exploited to tailor photo-crosslinked hydrogel systems. From a tissue engineering perspective, incorporation of GA within the hydrogel matrix is highly valuable as we found that grafting of GA to HA-gels impart an immunosuppressive microenvironment by polarizing macrophages to an immunosuppressive phenotype and also provide tissue adhesive characteristics [19].

In this work, we report the fabrication of blue light crosslinked HA-collagen hydrogels embedded with HA-coated carbon nanotubes (HA-MWCNTs). We could elegantly harness the radical forming capability of GA to crosslink HA and collagen wherein riboflavin was used as a biofriendly photosensitizer that enables fast crosslinking (within 5 min) when exposed to blue light of 405 nm wavelength, which is not harmful to cells. In addition, we incorporated HA-MWCNTs to enhance structural integrity of the hydrogel system, as we had previously shown that addition of CNTs to hydrogel scaffolds enhanced their conductivity and mechanical properties [29,30]. This novel hydrogel displayed excellent stability, cytocompatibility, antioxidant, and tissue adhesive properties while maintaining its shape without showing significant cell-mediated shrinkage upon fibroblasts or cardiomyocyte encapsulation and culture for one week. To assess the suitability of the bioink for tissue engineering, we monitored subcellular organization as well as contractile function and calcium handling properties of encapsulated hiPSC-cardiomyocytes. Finally, we 3D-bioprinted human fibroblasts-as well as hiPSC-cardiomyocyte-laden hydrogels and show high shape fidelity.

2. Experimental section

2.1. Carbon nanotube coating chemistry

Multiwalled carboxylic acid functionalized carbon nanotubes (755125-1G, Sigma Aldrich) were dispersed in deionized water with vigorous stirring and sonicated at 30 W with 60 % amplitude and 10 s on/off bursts with UP200St hierschler sonicator. EDC (03449-5G, Sigma Aldrich) chemistry was used to functionalize the carbon nanotube surface with carbodihydrazide (CDH) (C11006-100G, Sigma Aldrich) moieties, according to our previous report [29]. Briefly, CDH, 1-Hydroxbenzotriazole hydrate (HoBt) (54802-250G-F, Sigma Aldrich), and EDC were dissolved in the dispersion of multiwalled carbon nanotubes and left to stir vigorously overnight. EDC chemistry was followed with three days of dialysis using Spectrum™ Labs Spectra/Por™ 3 3.5 kD MWCO Standard dialysis membrane (Spectrum Labs 132725T). For the first 24 h, the solution was dialyzed against 2 L deionized water with 3 drops of 10 N Hydrochloric acid (HCl) and 12 g of Sodium Chloride (NaCl). The second day dialysis was performed against 3 drops of 10 N HCl in 2 L deionized water, and on the third day, dialysis against 2 L of deionized water alone with a minimum of 3 water changes per day. After dialysis, HA (100 kDa, Lifecore Biomedical Chaska Minnesota USA, HA100K-5) was dissolved into the dispersion and allowed to stir at 750 rounds per minute (rpm) overnight. HA physically and chemically coated the nanotubes via electrostatic charge difference and aldehyde carbohydrazide chemical crosslinking.

2.2. Gallic acid conjugation onto hyaluronic acid

GA -modified HA was prepared using previously reported EDC chemistry [19]. Briefly, HA (400 mg) and HoBt (1 mol equivalent 153 mg) were dissolved together in 75 mL deionized water with constant stirring. Gallic hydrazide (0.5 mol equivalent, 92 mg) prepared in house with previously reported chemistry [19] was dissolved in 25 mL dimethyl sulfoxide (DMSO) (10722164, Thermofisher Scientific) and then added dropwise to the stirring HA and HoBt solution. EDC cross-linker (0.25 mol equivalent, 48 mg) was added in two small batches 15 min apart and the mixture was left to stir overnight. HAGA was further dialyzed for three days against three drops of HCl (10 N) in deionized water (2 L) and NaCl (12 g) on day 1, three drops of HCl (10 N) in deionized water (2 L) on day 2, and against deionized water (2 L) alone on day 3 with a minimum of three water changes per day. After dialysis, HAGA was lyophilized and stored at −20 °C. UV–Vis and Proton ^{1}H NMR were used to confirm GA conjugation and percentage of modification (Figs. S1 and S2). UV–Vis spectroscopy was conducted by dissolving HA-GA in 1x phosphate-buffered saline (PBS) at a concentration of 1 mg/ml and measuring the absorbance within 240–340 nm. The standard curve of the commercial gallic acid was established over the concentration range of 10–200 μM. The degree of modification was found to be 10 mol% with respect to the repeated disaccharide units of HA. ^{1}H NMR further confirmed the 10 mol% conjugation of GA onto HA by the presence of distinctive aromatic peaks at 6.98 and 6.93 ppm of GA.

2.3. Hydrogel preparation

To prepare different hydrogel groups, a constant mass concentration of collagen I was maintained. As an example of the preparation, here the preparation of hydrogels with a volume of 150 μL is described. Table 1 outlines the specific volumes of stock solutions used to produce acellular or cell-laden hydrogels. Hydrogel precursors were prepared on ice. The following stock solutions were first prepared.

- Collagen I solution: 4.0 mg/mL (Advanced Biomatrix, 5153), a ready-to-use acidic solution.
- Riboflavin solution: 10 mg/mL in Dulbecco's PBS (DPBS, Sigma-Aldrich D8662).
- HA-coated MWCNTs: 2 mg/mL in deionized water.
- HAGA30 and HAGA60 stock solutions: Prepared by dissolving GA-modified HA directly into collagen I acidic solution (4.0 mg/mL) at 4 °C. The concentrations of GA-modified HA were 1.37 mg/mL for HAGA30 and 2.74 mg/mL for HAGA60, corresponding to ~30 % and ~60 % of the mass of collagen I in the final hydrogel precursor mixture, respectively (as shown in Table 1). To facilitate dissolution of GA-modified HA, 2 v% HCl (37 %) was added to the HAGA30 and HAGA60 solutions.

All components were kept on ice during hydrogel preparation except for the neutralization solution, which was at room temperature until mixing. When required for preparing the hydrogel precursor, the components were mixed in the following order: DPBS, MWCNTs, neutralization solution, collagen I solution or HAGA stock solutions, and eventually riboflavin. All hydrogel precursors and riboflavin stock solution were protected from light. The precursor solution was kept cold until use. For encapsulating cells, the hydrogel precursor solution was pipetted directly on top of the cell pellet of a known number of cells and gently mixed with pipetting avoiding bubble formation. The gel solution was pipetted into each well or mold and cured for 5 min of blue light exposure followed by incubation at 37 °C and 5 % CO_2 for 30 min. After photo-crosslinking, media was added to the wells, submerging the hydrogels.

Table 1
Constituent materials per each group of hydrogels (all volumes are μL).

Stock solution	collagen	collagen-riboflavin	HAGA0	HAGA30	HAGA60
collagen I solution	131.67	131.67	131.67	–	–
HAGA30 stock	–	–	–	131.67	–
HAGA60 stock	–	–	–	–	131.67
Neutralization solution	14.63	14.63	14.63	14.63	14.63
HA-coated MWCNTs	–	–	3	3	3
Riboflavin	–	0.18	–	0.18	0.36
DPBS	3.7	3.52	0.7	0.52	0.34
Total volume	150	150	150	150	150

2.4. Thermogravimetric analysis

Thermogravimetric Analysis (TGA) measurements were conducted with a TA Instruments q500 Thermogravimetric Analyzer. 10 mg of lyophilized HA-coated MWCNTs and uncoated MWCNTs directly from the bottle (755125-1G, Sigma Aldrich) were loaded onto the free hanging weigh pan. A temperature ramp from 25 °C to 1000 °C at 25 °C/min was conducted and the resulting weight of the pan measured every 0.5 °C. Measurements were conducted under an inert nitrogenous atmosphere with the sample gas flow at 60 mL/min and the balance gas flow at 40 mL/min.

2.5. Dynamic light scattering and surface zeta potential

HA-coated MWCNTs and CDH-conjugated MWCNTs were dispersed in deionized water at 0.25 mg/mL and sonicated with a UP200St Hielscher ultrasonic homogenizer at 30 W power, 20 % amplitude in 10 s on/off bursts while samples were on wet ice. 1 mL of solution was loaded into polystyrene cuvette and dynamic light scattering measurements were taken with a Malvern Zetasizer. For surface zeta potential analysis, 1 mL of solution at a reduced concentration of 0.1 mg/mL was added to polystyrene cuvette with universal zeta potential 'dip' cell kit placed into the solution provided by Malvern. Zeta potential measurements were carried out in zeta potential mode with a Malvern Zetasizer.

2.6. Rheological properties

A volume of 200 μL hydrogel precursor was prepared in 12 mm cylindrical molds and was exposed to 5 min blue light exposure followed by an incubation at 37 °C for 30 min. Their rheological properties were assessed with a TA instruments TRIOS Discovery HR 2 rheometer with a hot plate set to 37 °C and a solvent trap to emulate cell culture conditions. All measurements were conducted with 12 mm stainless steel parallel plate geometry. First, amplitude sweeps from 0.1 % to 20 % strain with a set frequency of 1 Hz were conducted to evaluate the linear viscoelastic region (LVER) to define the rheological stability of the gels and to assess the critical yield point. Next, frequency sweeps from 0.1 Hz to 10 Hz with a set 1 % oscillation strain within the LVER generated rheological fingerprints of the hydrogels. Additionally, amplitude and frequency sweeps were conducted at day 3 and day 15 of gels with CRL-2429 cells encapsulated following the shrinkage study protocol explained in section 4.10 below. The elastic storage modulus G' and the viscous loss modulus G" were evaluated across frequencies to determine the viscoelastic properties of the hydrogels. Further, time-dependent hydrogel crosslinking kinetics of 200 μL gel precursor solutions were measured and compared across groups using time sweeps at set 1 % oscillation strain and 1 Hz frequency with 60 s intervals of on/off blue light exposure and set 37 °C hot plate with a solvent trap to minimize drying. HAGA60 precursor bioink rheological characterization with 200 μL loaded volume was conducted at 10 °C unless otherwise indicated. Rheological bioink characterization included shear rate sweeps from 0.01 to 100 (1/s) to evaluate shear thinning characteristics at 10 °C, 37 °C, and 37 °C directly following 5 s blue light exposure. Thixotropy

analysis of HAGA60 bioink was conducted at 10 °C with 6 cyclic high (10/s) and low (0.01/s) sheer rate intervals of 60 s and resulting viscosity was measured over time. Oscillatory time sweeps were conducted to illustrate effectiveness of photo-induced crosslinking on cold 10 °C HAGA60 bioink with continuous blue light exposure initiated at 60 s. Finally, yield stress was estimated using Herschel-Bulkley fluid Model for non-Newtonian fluids following equation (1).

$$\tau = \tau_0 + K\left(\frac{du}{dy}\right)^n \tag{1}$$

Where $\frac{du}{dy}$ is the shear rate (or velocity gradient), τ represents the applied shear stress, τ_0 is the yield stress, K is the consistency coefficient, and n is the flow behavior index. Viscosity according to the Herschel Bulkley model can be described by the following equation (2).

$$\eta = \frac{\tau_0}{\left(\frac{du}{dy}\right)} + K\left(\frac{du}{dy}\right)^{n-1} \tag{2}$$

Power law curve fit was applied to shear rate sweep rheological data in excel to estimate yield stress τ_0, K, and n of HAGA60 bioink.

2.7. Electrical conductivity measurements

Electrical conductivity measurements were performed as explained previously [31]. Briefly, freshly mixed hydrogels (150 μL) were transferred into a self-built sealed polytetrafluoroethylene vessel and incubated at 37 °C for 30 min. By sweeping a bias voltage (±1.75 V) across the outer leads, two- and four-point current–voltage (I–V) characteristics were recorded. The values of the hydrogel electrical conductivity were estimated based on the four-point resistance values and accounting for appropriate geometrical corrections associated with the geometry of the measurement vessel [32]. During electrical characterization, samples were kept in a humid environment at a constant temperature of 37 °C. The measurements for each hydrogel were repeated at least three times.

2.8. DPPH radical scavenging assay antioxidant properties

The (2,2,1-diphenyl-1-picrylhydrazyl) DPPH (Sigma Aldrich, D9132-1G) method was employed to compare the radical scavenging properties of the hydrogels using a previously reported protocol [33]. Hydrogels (100 μL) were prepared in triplicate and cast into 24 well plates. DPPH stock solution was prepared by adding 4 mg of DPPH into 50 mL of 100 % ethanol and subsequently slowly diluted with more ethanol to adjust the absorbance of the DPPH stock solution to fall within the range of 1.08–1.12 arbitrary units (a.u.) absorbance maxima at 517 nm. A volume of 300 μL of the DPPH stock solution was pipetted on top of the crosslinked hydrogel samples in the 24 well plate and incubated for 30 min at room temperature. After 30 min of incubation, 100 μL of the DPPH solution was removed from the hydrogel samples and placed into a 96 well plate. Absorbance was measured and recorded at 517 nm using a Tecan Spark Multimode spectrophotometric microplate reader. The DPPH scavenging activity was calculated with the following equation.

$$\text{DPPH Scavenging activity } (\%) = \left[\frac{A_0 - A_1}{A_0}\right] \times 100 \tag{3}$$

A_0 refers to the blank stock DPPH solution absorbance used under the same reaction conditions without hydrogel samples, and A_1 equals the absorbance of the DPPH solution in the presence of the hydrogel samples. Absorbance background was corrected with 100 % ethanol blank wells without DPPH stock solution under the same experiment conditions. Results were the average of three independent measurements.

2.9. Tack adhesion test of hydrogels to porcine cardiac tissue

A tack adhesion test was performed with the TA instruments TRIOS Discovery HR 2 rheometer in axial mode to quantify the differences in the adhesive properties of the different hydrogel groups to cardiac tissue at 37 °C. Porcine cardiac tissue was prepared by slicing into an approximate 12 mm disc with 5 mm thickness with a surgical scalpel and super glued to the movable rheometer head (12 mm). Prior to super gluing, the rheometer metal head part was wrapped with wrapped tightly with a protective layer of (polytetrafluoroethylene) PTFE plumbers' tape to keep the metal clean from super glue. 200 μL molded 12 mm disc hydrogels were placed on the bottom rough steel plate underneath the head with the glued heart tissue. Subsequently, the heart tissue attached to the rheometer head was lowered into contact with the hydrogel sample and allowed to compress for 120 s (residence time) at a constant axial force of 100 mN to establish uniform molecular contact between the hydrogel and the heart tissue at 37 °C. Next, in axial mode, the rheometer head was pulled upwards at a constant velocity of 10 μm s^{-1} recording the axial force (N) with respect to time to illustrate the differences of cardiac tissue adhesion between the different hydrogel groups. Tests of each gel group were repeated in quintuples, and the average tack adhesion profile of each gel group was established and reported against step time along with the absolute average minimum force achieved of each gel group. The adhesion force corresponds to a negative axial force as the head pulls upwards, the gel and tissue adhesion pull downwards on the head, recording negative axial force (N) based on the adhesion strength between the heart tissue and the hydrogel.

2.10. Hydrogel shrinkage study

Human neonatal fibroblasts CRL-2429 cells were cultured in DMEM (Gibco DMEM with High glucose, GlutaMAX Supplement, pyruvate, Gibco™ 31966021) with 10 % fetal bovine serum (FBS) and 100 U penicillin and 100 μg Streptomycin (Pen/Strep). Cells were encapsulated into 200 μL hydrogels following hydrogel preparation steps for each group at a cell density of 2 million cells/mL (400,000 cells per 200 μL gel) and plated on top of non-adherent glass coverslip to study the full effect of internal cell traction without the gel material or encapsulated cells sticking to the bottom of the well plate. Gels were gently detached from the non-adherent sterile cover slip glass after crosslinking with a pipette tip to ensure no surface adhesion. Cells were grown in gels for 7–24 days. Media was changed every other day, and photos of gels were taken for each time point at 1 cm above the top of the plate using an Apple iPhone 12 main f/1.6 aperture 12 MP camera. NIH ImageJ was used to calculate the area of the gel in pixels at each time point, normalized to well size, and compared to the day 0 size to calculate shrinkage according to the following equation:

$$Area\,\% = \frac{Area}{Initial\ Area} * 100 \tag{4}$$

Rheological measurements of the gels with cells encapsulated was also carried out to evaluate mechanical changes over time at day 3 and day 15 of cell culture following rheology protocol outlined in section 4.6 above.

2.11. PrestoBlue and CyQUANT cell viability and proliferation assays

Dual PrestoBlue (Invitrogen, cat #A13262) cell viability assay followed by CyQUANT DNA quantification (Invitrogen, cat #C7026) were performed on 25 μL cell-laden hydrogel constructs with CRL-2429 fibroblasts encapsulated at a density of 2 million cells/mL (50,000 cells per 25 μL gel) following manufacturer's protocols as end point assay at each time point. Briefly, 25 μL cell-laden constructs were fabricated as described above in 24 well plates. Smaller gel volumes with same cell density were chosen to ensure cell numbers fit within assay's sensitivity

ranges throughout the experiment. PrestoBlue reagent was prepared by diluting 1:10 into cell media, normal cell media was removed and replaced with 500 μL PrestoBlue containing media per well. Constructs were incubated for 1 h in PrestoBlue media at each time point. 1 h incubation was selected to increase sensitivity of assay and allow for proper diffusion of dye throughout gel constructs. PrestoBlue containing media was then removed and placed into 96 well clear bottom black plate along with background blank PrestoBlue media. Fluorescence was measured using VICTOR Nivo multimode microplate reader with excitation wavelength set to 544 nm and emission wavelength of 595 nm. Data was background corrected at each time point with wells containing blank PrestoBlue media. Results presented as average of 3 independent biological replicate wells at each timepoint. Following PrestoBlue media removal to prepare samples for CyQUANT, gel constructs were soaked in 1x PBS for 15 min and washed 3x to remove any phenol red from DMEM and any remaining PrestoBlue dye that may interfere with CyQUANT signal. Gels were then removed from wells, placed in 1.5 mL plastic Eppendorf tubes, and submerged in sterile 1x PBS enzyme solution containing 500 U/mL collagenase type II (Gibco, cat #17101015) and 500 U/mL hyaluronidase (Sigma Aldrich, H3506-100 MG). They were then incubated for 1 h at 37 °C to gently break down gel materials and release encapsulated cells. Once gel materials were dissolved, samples were centrifuged at 1500 rpm for 5 min to form cell pellets. Enzyme solution was gently removed, and cell pellets were frozen at −80 °C. Once all time points were collected and frozen at least for 24 h, CyQUANT was performed on all samples on the same day. Briefly, extended linear range (250,000 cell upper limit) 5x CyQUANT working solution was prepared by diluting reagent 80-fold in 1x cell lysis buffer as described by manufacturer. 200 μL of CyQUANT working solution was added to each cell pellet, mixed, and pipetted into black clear bottom 96 well plates. Samples were incubated at room temperature for 5 min protected from light and subsequently the fluorescence was measured with VICTOR Nivo Multimode plate reader with emission wavelength of 480 nm and excitation wavelength of 530 nm. No cell blank 5x CyQUANT working solution controls were used to background correct signals, and data represents the average of 3 independent biological replicates at each time point.

2.12. Degradation performance

Blank 3 cm sterile petri dishes were individually labeled and weighed. Next, 100 μL sterile blank gels of each group were pipetted and crosslinked as previously described above separately in 3 cm sterile cell culture petri dishes. Whole Petri dish containing crosslinked gels were then weighed again prior to adding solutions for day 0 weight. Gels were submerged in 3 mL of either sterile 1x PBS, complete DMEM cell media (DMEM with 10 % FBS and Pen/Strep), 0.2 μm sterile filtered hyaluronidase solution (50 U/mL in 1x PBS), 0.2 μm sterile filtered collagenase type II solution (50 U/mL in 1x PBS), or 0.2 μm sterile filtered enzyme mix solution (50 U/mL of each Hyaluronidase and Collagenase type II in 1x PBS). Samples were incubated in cell incubator at 37 °C up to 28 days. At every time point, solutions were completely and gently removed, and whole Petri dish samples were massed. Once massed, fresh solutions were reapplied. Blank Petri dish weight was subtracted and weight % was calculated using equation (5) below. Data is representative average weight % of 3 individual replicates at each time point.

$$Weight\ \% = \frac{Gel\ weight}{Initial\ Gel\ Weight} * 100 \quad (5)$$

2.13. Scanning electron microscopy

Scanning electron microscopy (SEM) was performed as described previously [31]. Briefly, hydrogels were fixed in a 1:1 mixture of glutaraldehyde and paraformaldehyde (3.7 %) for 1 h, followed by gradual dehydration in ethanol series (10 %, 20 %, 30 %, 50 %, 70 %, 80 %, 90 %, 95 %, and 100 %), with each step lasting 30 min, followed by immersion in 100 % ethanol. Subsequently, samples were critical point dried using an EM CPD300 (Leica, 12 cycles, exchange speed of 5 and 120 s delay) and sputter-coated with gold for 30 s (Q150T, Quorum Technologies Ltd., Germany). Scanning electron microscopy (FE-SEM, Auriga, Carl-Zeiss, Germany) was performed on the cross-sectional area of the samples.

2.14. Cardiac differentiation of hiPSCs

F1 hiPSCs at passage number 24–29 were differentiated in cardiomyocytes based on an established method [34]. Briefly, mesoderm formation through activating Wnt signaling was induced in hiPSCs more than 85 % confluent by introducing CHIR-99021 (6 μM) for 2 days. After 1 day of incubation in the culture medium, Wnt signaling was inhibited by IWR-1-endo (5 μM) for 2 days. After another 2 days of incubation in a culture medium, cells started to beat. Up to this point, the basal differentiation medium was RPMI 1640 containing B-27 supplement minus insulin (2 %, Thermo Fisher Scientific, A1895601). Subsequently, cells were cultured for 2 days in RPMI 1640 supplemented with B-27 supplement (2%, Thermo Fisher Scientific, 17504044), and on day 9 of differentiation, cells were cultured in RPMI 1540 without glucose supplemented with sodium DL-Lactate (4 mM, Sigma Aldrich L7900) to purify cardiomyocytes for 2 days. The resulting cells were then cultured in RPMI 1640 supplemented with B-27 supplement (2%).

2.15. Generation of engineered tissues

The pre-gel solution of collagen, collagen-riboflavin, HAGA0, HAGA30, or HAGA60 hydrogels was prepared according to Table 1. For engineered cardiac tissues, 2.5×10^7 cells/mL were resuspended in the pre-gel solution. The cell-laden hydrogels (15 μL) were dispensed in each well of a 24 well plate, were exposed to a blue light source with a wavelength of 405 nm at the intensity of 90 % for 8 min. After that, the samples were placed in a cell culture incubator at 37 °C and 5 % CO_2 for 30 min to induce thermal gel formation. Tissue constructs were incubated in RPMI 1640 supplemented with B-27. The same procedure was performed to generate fibroblast-based tissues with a cell density of 2×10^6 cells/mL of CRL-2429 fibroblasts. These cells were then cultured in DMEM/F12 supplemented with 10 % FBS and Pen/Strep.

2.16. Live/dead assay

The viability of cells in tissue constructs was determined using a Live/Dead viability/cytotoxicity kit (L3224, Invitrogen) [34] and quantified using NIH ImageJ software. Briefly, calcein-AM (0.025 %) and EthD-1 (0.1 %) were diluted in DPBS and added to each tissue followed by 15 min incubation in an incubator at 37 °C and 5 % CO_2. For the CRL-2429 containing samples in shrinkage studies (Fig. 5a), samples were imaged using Nikon Ts2 inverted epi-fluorescent microscope directly after incubation in place at bottom of well. For hiPSC cardiomyocyte-containing hydrogels, the tissue samples were mounted on a microscopy slide without mounting medium but with a cover slide and immediately imaged using a Zeiss LSM-800 confocal laser scanning microscope.

2.17. Immunostaining analysis

Tissue constructs were immunostained for cardiac or fibroblast-specific markers as previously described [35] with the following modifications. Samples were fixed in paraformaldehyde (3.7 %) for 30 min and permeabilized in Triton X-100 (0.25 %) for 20 min. The following primary antibodies were used for overnight incubation at 4 °C: for cardiac tissues: mouse anti-sarcomeric α-actinin (1:250, Abcam, ab9465), rabbit anti-connexin43 (1:250, Abcam, ab11370) and goat anti-cardiac troponin I (1:250, Abcam, ab56357). For fibroblast tissues:

rabbit anti-vimentin (1:250, Abcam, ab92547). The following secondary antibodies were used for 2 h incubation at room temperature in the dark: donkey anti-mouse AlexaFluor 488 (1:500, Abcam A21202), donkey anti-rabbit AlexaFluor 594 (1:500, Abcam A-21203), and donkey anti-goat AlexaFluor 647 (1:500, Abcam A-21081). DNA was visualized with 4′,6-diamidino-2-phenylindole (DAPI, 0.5 g/mL in 0.1 w/v% NP40, 15 min). In the end, samples were mounted with a fluorescent mounting medium and preserved for microscopy.

2.18. Calcium handling of cardiac tissues

Analysis of calcium handling of engineered cardiac tissues were performed using Fluo-4 Direct™ Calcium Assay Kit (ThermoFisher Scientific), as described previously [34]. Following the manufacturer's instructions, tissue constructs were incubated for 60 min with the labeling solution diluted in culture media (1:3 dilution). Subsequently, the fluorescent movies were acquired using a live cell imaging setup (Keyence Microscopy) with a 4× objective and a GFP filter at 488 nm.

2.19. Preparation of support bath

The two-component support bath of gelatin-gum arabic was prepared according to our previously published protocol [27].

2.20. 3D bioprinting

A bioink of HAGA60 was prepared as explained in "4.2 Hydrogel preparation". CRL-2429 fibroblasts or hiPSC-cardiomyocytes were harvested from culture plates, centrifuged, and resuspended in the gel precursor of HAGA60 by carefully pipetting up and down using a 1 mL pipet. The cell-laden bioink was transferred into a 5 mL syringe and placed into the cartridge of an Allevi 3 bioprinter. In parallel, the support bath was prepared and poured into an appropriate vessel using a 1 mL pipet. A 3D design of a ring with the diameter of 10 mm, height of 1 mm, and filament thickness of 0.1 mm was generated in license-free Autodesk Tinkercad platform, and the stl file was imported into an Allevi 3 bioprinter. For cardiac ventricles, a 3D design was made in Blender, and two ventricle shapes were designed as a small ventricle opening (size 5 mm × 5 mm x 5.21 mm (X:Y:Z)) and a big ventricle opening (5 mm × 5 mm x 4 mm (X:Y:Z)). Printing was executed at a cartridge temperature of 4 °C, print speed of 6 mm/s, layer height of 0.4 mm, and a pressure of 1.0 psi for the rings. To print the ventricles, a cartridge temperature of 15 °C, print speed of 6 mm/s, layer height of 0.2 mm, and extrusion pressure of 1.0 psi was used. After the 3D printing step, samples were exposed to blue light at 405 nm at 90 % intensity for 5 min. Then, tissues were placed in an incubator at 37 °C and 5 % CO_2 for 30 min, during which the support bath was melted and replaced with fresh DMEM/F12 supplemented with 10 % FBS and Pen/Strep for fibroblast-laden rings. For 3D-bioprinted ventricle models, the support bath was replaced with Iscove's medium supplemented with B27 supplement minus insulin (4 %), IGF-1 (10 ng/mL), FGF-2 (10 ng/mL), VEGF165 (5 ng/mL), non-essential amino acids (1 %), and Pen/Strep.

2.21. Movie acquisition

Movies of beating 3D constructs and movies for calcium handling assays were recorded in wells of 24 well plates for 10 s. All movies were recorded under a Keyence BZ9000 microscope. Calcium movies were analyzed, as explained previously, over four different regions of interest per movie [34]. Movies of beating 3D-bioprinted ventricles were recorded using a high-speed camera on ZEISS Axio Zoom.V16 Stereomicroscope and exported as avi files.

2.22. Microscopy

Fluorescence images for Live/Dead viability studies in the shrinkage assay (Fig. 5a) with encapsulated CRL-2429 fibroblasts were acquired using a Nikon ECLIPSE Ts2 inverted epi-fluorescent microscope. The same LED illuminator power and settings were used for all presented images. For calcein AM imaging, excitation wavelength was set to 470 nm and for EthD-1, excitation was set to 560 nm. All other fluorescence images were acquired on an LSM 800 confocal laser scanning microscope (Carl Zeiss). The same laser power and settings were used for all presented images within individual assays. The following excitation and emission wavelengths were set for each secondary antibody: AlexaFluor 488 (excitation 493 nm, emission 517 nm, detection wavelength 450–585 nm), AlexaFluor 594 (excitation 280 nm, emission 618 nm, detection wavelength 595–650 nm), AlexaFluor 647 (excitation 653 nm, emission 668 nm, detection wavelength 645–700 nm), DAPI (excitation 353 nm, emission 465 nm, detection wavelength 410–546 nm). The pinhole was set to 1 airy unit.

2.23. Statistical analyses

Data from at least three independent experiments were expressed as mean ± standard deviation (SD). Statistical significance of differences was evaluated by a two-tailed Student's t-test (GraphPad Prism) or, where appropriate, by one-way or two-way analysis of variance (ANOVA) followed by Bonferroni's posthoc test (GraphPad Prism) unless otherwise indicated in the manuscript. Data are presented as mean ± standard deviation (SD). Significant differences were indicated by *: $p \leq 0.05$, **: $p \leq 0.01$, ***: $p \leq 0.001$, and ****: $p \leq 0.0001$.

3. Results and discussion

3.1. Modification of MWCNTs and hydrogel formation

In order to generate hydrogels based on GA-functionalized HA (HAGA), collagen I, and HA-MWCNTs, we first synthesized hydrazide-functionalized MWCNTs by conjugating carbodihydrazide onto carboxylic acid-functionalized MWCNTs using EDC chemistry, according to our previously published protocol [29,30]. These nanotubes were then coated with unmodified HA through electrostatic adhesion forces between positively charged hydrazide functional groups of MWCNTs and the negatively charged HA molecules (Fig. 1a). HA was selected as the coating material to improve dispersibility of the MWCNTs in solution. We used TGA analysis to evaluate a successful HA coating of the MWCNTs (Fig. 1b). The analysis of TGA showed a continuous and faster decrease in the mass of the HA-MWCNTs compared to the uncoated MWCNTs, indicating a thermal degradation of HA over increased temperatures, confirming the successful coating of MWCNTs with HA. Analysis of the size of nanotubes using dynamic light scattering (DLS) revealed an increased average hydrodynamic size of nanotubes from ~100 nm for uncoated MWCNTs to ~500 nm for HA-MWCNTs (Fig. 1c). Further analysis of nanotubes surface charge by zeta potential measurements showed a shift towards more negative charges after particles being coated with HA, further providing evidence of a successful coating of MWCNTs.

To form a hydrogel, we mixed rat tail collagen I with the HA-MWCNTs and dissolved HAGA at different concentrations directly into acidic collagen I solution. The HAGA was synthesized following our reported protocol [17,19]. The degree of GA modification was estimated to be 14.6 mol% based on the UV measurement (Fig. S1). The degree of modification was further corroborated by ^{1}H NMR (in D_2O), which displayed 15 mol% of GA modification with respect to the disaccharide repeat units of HA as estimated by integrating aromatic peaks at 6.85 ppm of GA with N-acetyl signal of HA at 1.829 ppm (Fig. S2). We utilized vitamin B2 (riboflavin) as a photosensitizer for crosslinking GA and collagen I. The hydrogel was fabricated by mixing appropriate amounts of HAGA, collagen I, riboflavin, and MWCNT-HA, as presented in Table 1, with blue light exposure (5 min), followed by incubation at 37 °C for 30 min (Fig. 1e). We designed material groups to study the

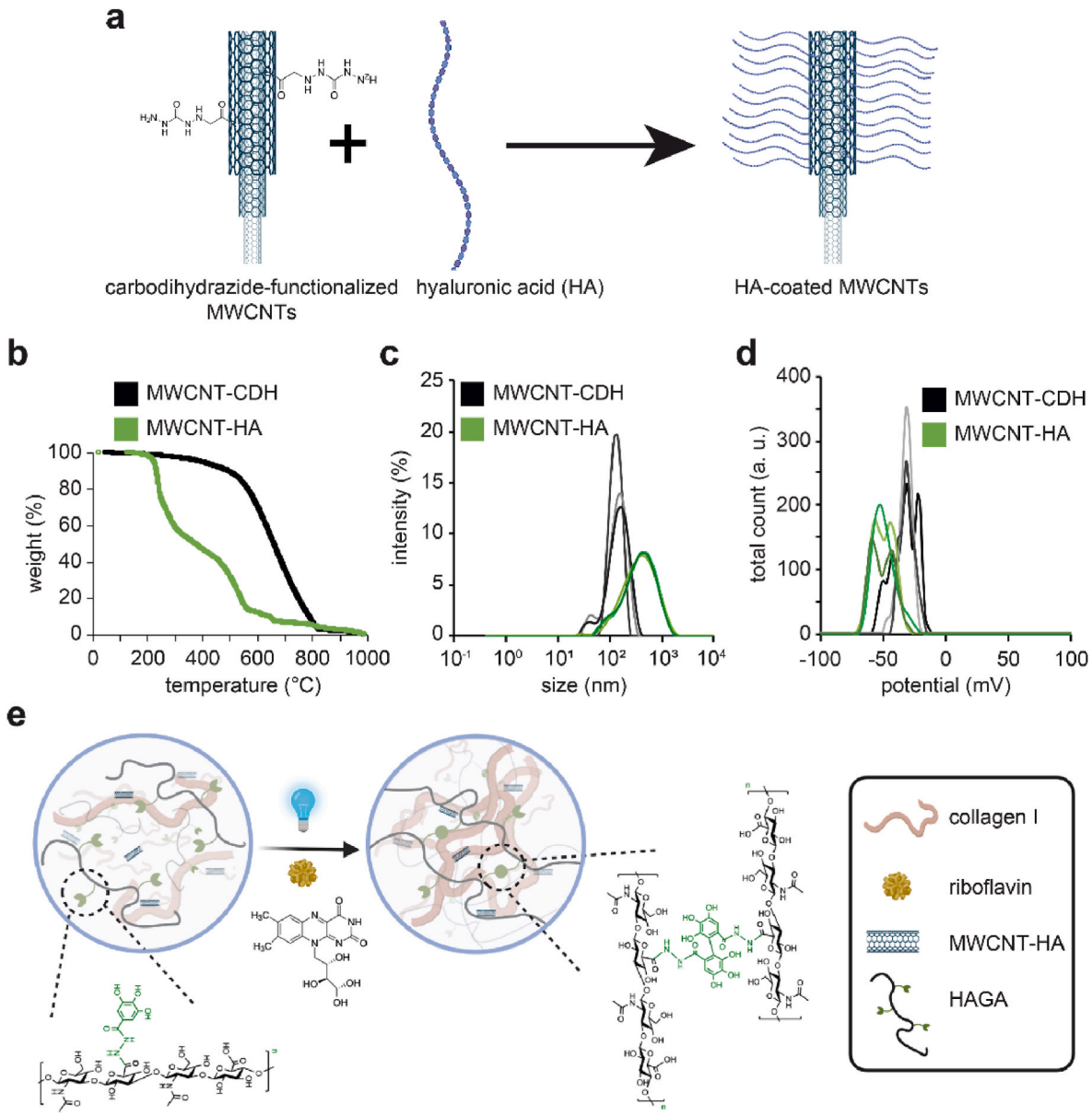

Fig. 1. Materials modification and hydrogel formulation. (a) Schematic illustration of carbon nanotube coating with hyaluronic acid (HA). (b) Thermogravimetric analysis of uncoated and HA-carbon nanotubes. Dynamic light scattering analysis of carbon nanotubes reporting (c) size and (d) surface (zeta) potential. (e) Schematic illustration of hydrogel formation based on collagen I, hyaluronic acid, and HA-MWCNTs. In **d**, a.u. indicates the arbitrary units.

addition of each component to collagen I and compared each group to collagen I hydrogels as the control. All groups contained equal mass weight of collagen I.

We added riboflavin to collagen I alone to form the collagen-riboflavin group, HA-MWCNTs to collagen I to elucidate the effect of adding the HA-MWCNTs forming the HAGA0 group. Subsequently, we mixed all components together, adding increasing amounts of HAGA at 30 % by weight of collagen content in the HAGA30 group, and 60 % of collagen content by weight in the HAGA60 group to compare the effects of adding HAGA to the system at increasing amounts. The addition of HAGA into the system along with riboflavin was evaluated and compared to collagen I alone with and without HA-MWCNTs throughout the study. HAGA30 and HAGA60 hydrogels benefit from a double crosslinking strategy forming an interpenetrating network, namely (i) GA-mediated photo-crosslinking and (ii) thermal self-assembly of collagen fibrils.

3.2. HAGA inclusion to collagen I hydrogels retains fibrillar structure and enhances conductivity

We performed a series of experiments to assess the effect of HAGA addition to collagen I hydrogels. To evaluate the microstructure of the hydrogels, SEM was performed on sputter-coated samples of critical point dried hydrogels (Fig. 2a). Analysis of SEM images confirmed a fibrillar structure of all hydrogels. In addition, we studied whether the addition of HA-coated MWCNTs increases the electrical conductivity of the hydrogels based on four-point-probe (Fig. 2b) and two-point-probe (Fig. 2c) analyses. Previously, we had shown that hydrazide-functionalized MWCNTs improve electrical conductivity and that electrically conductive materials enhance electrical coupling and maturation of cardiomyocytes in engineered cardiac tissues [30,31,34,36,37]. These measurements revealed a conductivity of 144.3 ± 6.3 mS/cm for collagen I hydrogels (Table 2).

Inclusion of riboflavin into collagen I hydrogels did not significantly alter the conductivity resulting in 139.6 ± 1.5 mS/cm. Including HA-

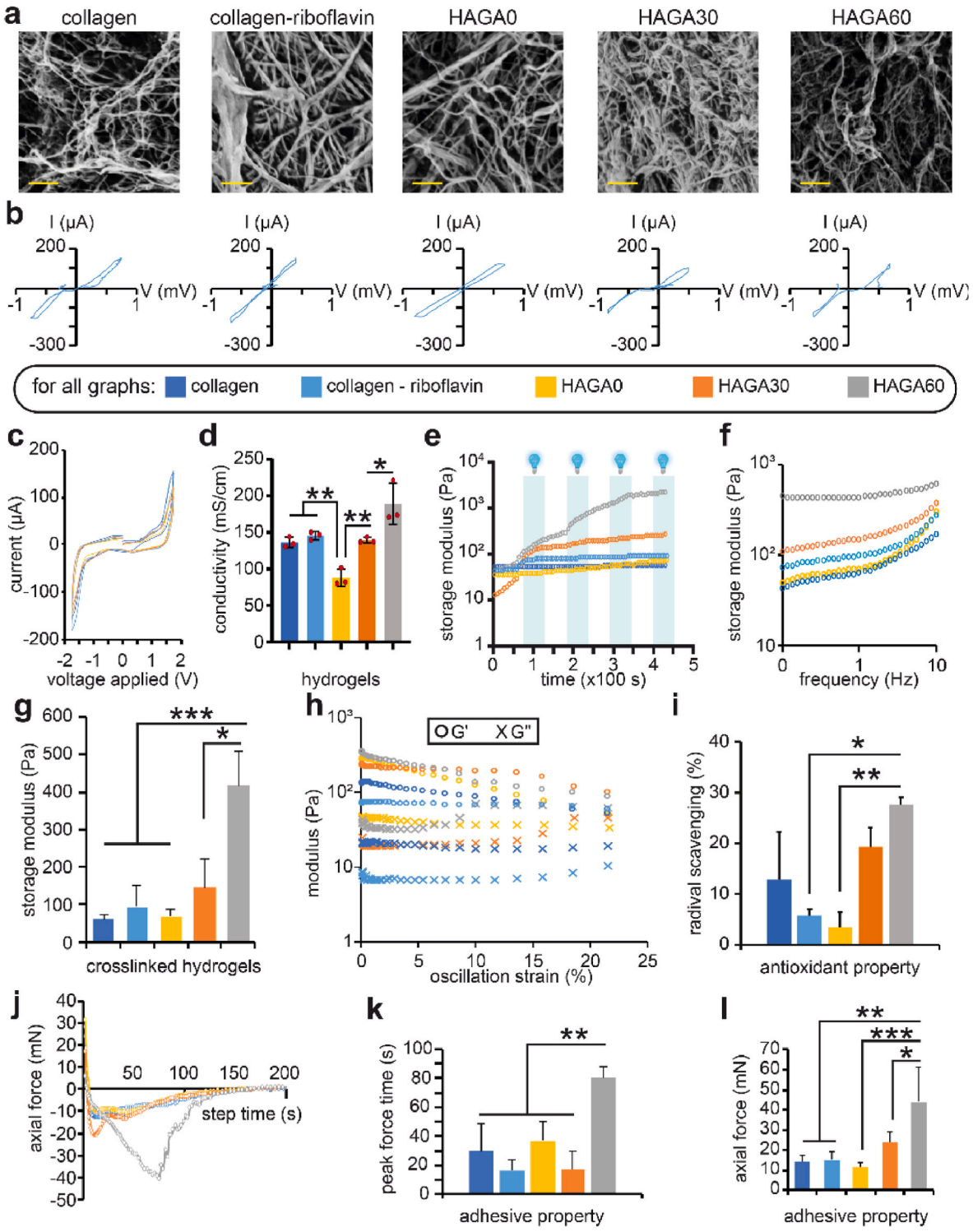

Fig. 2. Hydrogel characterization. (a) Representative scanning electron microscopy images of critical point dried hydrogels. (b) Representative I–V graphs of conductivity measurements of hydrogels based on four-point-probe and (c) two-point analysis. (d) Conductivity values calculated based on four-point-probe analysis (n = 3). (e) Evolution of storage modulus of hydrogels over time, based on time sweep analysis. (f) Evolution of storage modulus G' (Pa) of hydrogels based on frequency sweep analysis. (g) Storage modulus at 1 Hz frequency of hydrogels extracted from frequency sweep analysis. (h) Evolution of shear modulus (G′ Storage Modulus and G″ Loss modulus) of hydrogels at different oscillation strain % based on amplitude sweep test. (i) Quantitative analysis of antioxidant properties of hydrogels (n = 3). (j to l) Quantitative analysis of (j) adhesion properties over time (n = 3), (k) time to reach the peak force for detachment (n = 3), and (l) force required for detachment (n = 3). Data is mean ± SD. One-way ANOVA with Bonferroni's posthoc analysis was performed. Scale bar: 100 μm.

Table 2
Electrical conductivity of hydrogels.

Material	Conductivity (mS/cm)
collagen I	144.3 ± 6.3
collagen-riboflavin	139.6 ± 1.5
HAGA0	82.1 ± 0.6
HAGA30	143.9 ± 2.9
HAGA60	221.7 ± 13.3

coated MWCNTs into collagen I hydrogels resulted in decreased conductivity values of 82.1 ± 0.6 mS/cm. However, the decreased conductivity of HAGA0 was elevated when incorporating HAGA, resulting in 143.9 ± 2.9 mS/cm in HAGA30. Conductivity was further increased by increasing the amount of HAGA, reaching 221.7 ± 13.3 mS/cm in HAGA60, a higher electroconductivity than that of plain collagen I hydrogels (Table 2 and Fig. 2d).

The presence of carbon nanotubes in collagen I hydrogels is known to enhance conductivity of hydrogel constructs [38]. Nevertheless, we observed that the presence of HA-coated MWCNTs resulted in lower conductivity compared to that of collagen I. This phenomenon is probably due to steric hindrance induced by the HA coating that might interfere with the charge propagation through the matrix. Increased conductivity in hydrogels containing HAGA could be due to π-π stacking between GA and the exposed aromatic surfaces of the MWCNTs. It has been shown that GA increases conductivity of hydrogels owing to π-π stacking and increased interfacial adhesion between the electrode surface and polymer networks [39].

3.3. HA-MWCNTs and HAGA inclusion enhances mechanical properties of the hydrogels

Hydrogel mechanics play a significant role in the stability and corresponding biological functions of encapsulated cells within constructs. Mimicking native ECM with our hydrogels aims at providing encapsulated cells with natural mechanical cues, thus we measured and compared the bulk hydrogel mechanics as well as gelation kinetics [40]. We believe the radical generating property of gallol moiety on the HAGA and nucleophilic reactive groups within collagen I chains covalently bind together after activation by riboflavin under blue light, further increasing crosslinking of the system and reinforcing the matrix. In order to study the gelation kinetics of the hydrogels, gel precursor of each composition was placed onto the lower geometry of a TA instruments TRIOS Discovery HR 2 rheometer, and a time sweep assay at a fixed 1 Hz frequency and 1 % oscillation strain was performed at 37 °C, measuring the storage (G′) and loss moduli (G″) over time with sequential 60 s on/off cycles of blue light exposure (Fig. 2 e). Analysis of time-sweep rheometric data revealed that with the addition of HAGA, the gel constructs continued to be light-responsive after repeated light exposure time frames, evidenced by a continuous increase of storage modulus G' from 0 Pa to 1000 Pa after 180 s of combined blue light exposure (Fig. 2e). The continuation of light responsiveness and increasing stiffness upon repeated light exposure of HAGA30 and HAGA60 groups provides evidence towards the added reactivity of HAGA inclusion into the gel system. To generate our hydrogels, we performed photo-crosslinking before 37 °C incubation to ensure faster covalent crosslinking between GA-modified HA and free polymeric chains of collagen I. This method ensures a quick stabilization of the hydrogel structure, especially during 3D printing, as shown in Fig. 2d and 6b.

Previous work has illustrated that riboflavin can be used in combination with UV or blue light to crosslink collagen alone in connective tissues and collagen hydrogels [17,18], however, this crosslinking is weak resulting in modest enhancement of mechanical properties of the hydrogel. For example, the exposure of collagen to blue light in the presence of riboflavin increased the storage modulus from 5.28 ± 2.03 Pa to 8.82 ± 0.72 Pa after 1 min irradiation [37]. Here, we have also observed similar results. The collagen I hydrogel exhibited a storage modulus of 92 Pa, and irradiation of collagen I hydrogels with blue light in the presence of riboflavin showed only a modest enhancement of mechanical properties to 127 Pa at 1 Hz frequency and 1 % oscillation strain (Fig. 2f and g). In contrast, incorporation of HAGA had a profound impact on the viscoelasticity and stability of the hydrogel. The inclusion of HAGA resulted in an increased storage modulus (G′) and a higher strain stiffening with increasing frequencies compared to native collagen I (at day 0 at 1 Hz frequency; collagen: 92 ± 67 Pa vs. HAGA30: 198 ± 61 Pa vs. HAGA60: 378 ± 133 Pa, Fig. 2f and g). At 10 Hz frequency, there was a threefold increase in the storage modulus (G′) to 663 Pa for HAGA60 compared to 251 Pa for collagen I when the HAGA was crosslinked at 405 nm light exposure for 15 s. To determine the role of MWCNTs, we assessed the storage modulus of HAGA60 with and without MWCNTs. In addition, we utilized unmodified HA to validate the effect of GA-functionalization of HA on the storage modulus (Figs. S3a and b). Our data showed that the presence of MWCNTs results in an increased storage modulus of HAGA60. In addition, the storage modulus of hydrogels with unmodified HA was markedly lower than HAGA60 confirming the role of GA for crosslinking. The amplitude sweep analysis (Fig. 2h) showed that the groups without HAGA incorporated (native collagen I group along with collagen I-riboflavin and HAGA0 groups) have lower storage moduli with G′ for native collagen I ranging from 136 Pa to 53 Pa compared with G′ for HAGA30 ranging from 237 Pa to 99 Pa, and G′ for HAGA60 ranging from 363 Pa to 88 Pa over the same linear viscoelastic region. These values are greater than the storage moduli reported previously for collagen-based engineered cardiac tissues (20–30 Pa) [41], however, they are significantly softer than ≈10 kPa reported for the end-diastolic shear storage modulus of human myocardium [42]. For all groups, non-linear properties began to appear at ~15 % oscillation strain, and gels began to lose their elastic solid structure. The exact storage (G') and loss (G") moduli values derived from the frequency sweeps at 1 Hz frequency and 1 % oscillation strain is presented in Table 3. Notably, the storage modulus increases with increasing frequency. This is in agreement with the fact that mechanical loading of collagen I increases the toughness of collagen fibrils [43]. On the contrary, we have earlier shown that HA hydrogels become softer with mechanical loading [44]. At higher frequencies, we observed a strain-hardening effect of collagen I hydrogels and HAGA30 and HAG60 hydrogels which are attributed to the denser packing of collagen fibrils upon compression. Such strain-stiffening behavior matches native cardiac tissue. Interestingly, covalent crosslinking of the GA-functionalized HA to collagen I did not disrupt this behavior, suggesting that the HAGA30 and HAGA60 hydrogels retain the physiochemical characteristics of the native collagen I hydrogels while mitigating the matrix shrinkage induced by encapsulated cells.

In order to determine if the different hydrogels exhibit different balance in their viscous and elastic characteristics, we calculated loss tangent (Tan δ), which is a ratio of loss modulus (G″) to storage modulus (G') and shows whether a material behaves liquid-like (Tan $\delta > 1$) or solid-like (Tan $\delta < 1$). The Tan δ values at 1 Hz indicated that all gel groups exhibited solid-like (elastic) behavior as Tan δ was for all groups less than 1 (Table 3). Collagen I-riboflavin group exhibited the most plastic behavior with a Tan δ of 0.29 and HAGA0 exhibited the most solid-like behavior with a Tan δ of 0.0653. As loss tangent indicates the

Table 3
Rheological properties summary of collagen I – HAGA hydrogels at 1 Hz frequency.

Groups	n	G' (Pa)	G" (Pa)	Tan δ (G"/G′)
collagen I	5	91.77 ± 63.23	11.23 ± 5.17	0.1224
collagen-riboflavin	5	127.17 ± 83.05	36.49 ± 15.43	0.2869
HAGA0	5	155.57 ± 114.16	10.16 ± 2.86	0.0653
HAGA30	5	198.67 ± 60.79	31.82 ± 6.97	0.1602
HAGA60	5	378.00 ± 133.16	44.50 ± 22.26	0.1177

dampening effect of the hydrogels, this is particularly of interest in the context of cardiac tissue engineering as less dampening can translate into more efficient transduction of cell-generated forces, which is desirable in cardiac tissue engineering.

The amplitude sweep (Fig. 2h) was further used to determine the linear viscoelastic region, and the gels maintained solid structure, where G' was greater than G", with some non-linear effects due to the formation of possible microcracks appearing between 15 and 20 % oscillation strain without any gel groups reaching critical failure point by 20 % oscillation strain. Notably, to the best of our knowledge, no work has shown the addition of HAGA and blue light photo-crosslinking as a reinforcing agent and that the crosslinking of HAGA with collagen greatly enhances the viscoelasticity and stability of the hydrogel that supports cell survival and function.

In order to assess the degradability of the hydrogels, we studied their swelling and degradation behavior in PBS, DMEM complete culture medium, solutions of collagenase, hyaluronidase, and a mixture of collagenase and hyaluronidase (Fig. S4). Our data revealed that all hydrogels were swelling but not degrading in either PBS or DMEM culture media over 30 days, which was expected due to crosslinking of collagen I and, in the case of HAGA hydrogels the chemical crosslinking due to photocuring of the hydrogel precursor (Figs. S4a and b). Likewise, incubation of hydrogels in hyaluronidase for up to 8 days did not result in their degradation but only induced swelling. This suggests that the collagen I network strongly stabilizes the hydrogel structure. However, incubating hydrogels in collagenase or a combination of collagenase and hyaluronidase resulted in complete degradation of all hydrogels in 8 days (Figs. S4d and e).

3.4. HAGA inclusion into collagen I hydrogels increases radical scavenging and tissue adhesiveness

Due to the known ability of gallol moiety to act as a radical scavenger, we additionally quantified the radical scavenging ability of each hydrogel. The radical scavenging ability of the hydrogels was measured using a 2,2′-diphenyl-1-picrylhydrazyl (DPPH) radical scavenging assay (Fig. 2i). The radical scavenging capability of the hydrogels significantly increased by ~15 % with the inclusion of HAGA as compared to pure collagen I hydrogels. This indicates that the inclusion of HAGA imparts antioxidant and radical scavenging capabilities to the hydrogels.

For the successful implantation of hydrogels as cardiac patch, skin patch or other tissue engineering applications, it is of great advantage when biofabricated hydrogels exhibit tissue adhesive properties. Thus, we estimated the adhesive properties of our hydrogel to porcine cardiac tissue using the tack adhesion test on the rheometer based on adhesion properties over time (Fig. 2j), the time to reach the peak force for detachment (Fig. 2k), and the force required for detachment (Fig. 2l). The results revealed that HAGA inclusion significantly enhances the tack adhesion force to cardiac tissue by a factor of ~4 as well as the retention time of the hydrogel to the tissue interface with an elongated time to minimum force peak. This ability to adhere to cardiac tissue supports the possibilities for HAGA-containing hydrogels to be used as cardiac patches.

3.5. HAGA-collagen I-based hydrogels are suitable for cardiac tissue engineering

Cardiovascular diseases are the most common cause of death in the world [45] and currently, heart transplantation remains the only available therapy to restore heart function. Furthermore, congenital heart diseases are the leading cause of child mortality among birth defects and represent the most common congenital abnormalities (~1 % of all live births) [46]. In search of novel therapeutic strategies, engineered cardiac tissues are valuable tools to model disease and study drug response. In addition, pre-clinical animal studies suggest that transplantation of such engineered tissues can improve heart function after infarction [47–50]. The safety and efficacy of such a procedure for patients is currently being investigated in a clinical trial (ClinicalTrials.gov Identifier: NCT04396899). To determine if the here developed hydrogel system is compatible with hiPSC-cardiomyocytes, these cells were mixed at 2.5×10^7 cells/mL with either of the gel precursors, exposed to blue light (405 nm, 5 min), and subsequently incubated at 37 °C for 30 min. Confocal images of Live/Dead staining analysis at 7 days demonstrated the survival of hiPSC-cardiomyocytes in culture (Fig. 3a and b). Our data revealed that the addition of riboflavin or HA-MWCNT to collagen I did not induce cytotoxicity. Importantly, the chemical modification of HA, MWCNTs, and the photo-crosslinking of the hydrogels did not induce cell death in the hydrogels compared to collagen I alone (Fig. 3b), indicating cytocompatibility of the hydrogels. Immunofluorescence analysis of confocal laser scanning microscopic images of hiPSC-cardiomyocytes embedded within different hydrogels revealed that these cells spread in all hydrogels. Furthermore, hiPSC-cardiomyocytes exhibited clear sarcomeres (Fig. 3c), whereby parallel aligned myofibrils suggested a proper formation of their contractile machinery (Fig. 3c). Quantitative analysis of connexin 43 (Cx43) showed no significant differences (Fig. 3d) and the sarcomeric length of cardiomyocytes correlated with increasing HAGA concentrations, indicating improved maturation (Fig. 3e). However, the difference in sarcomeric length was not significant. These data show that the here developed hydrogels provide a suitable environment for hiPSC-cardiomyocytes.

To assess whether our hydrogel allows proper electrical coupling of cardiomyocytes and permits seamless intercellular communications, we labeled hiPSC-cardiomyocytes in the different types of hydrogels with calcium-sensitive dye Fluo-4 (37 °C, 60 min) and performed live cell imaging using a Keyence BZ-9000 fluorescent microscope. Subsequent quantitative analysis of recorded videos (10 s) revealed a synchronous homogenous calcium wave in all engineered tissues (Fig. 4, Movie S1).

Spontaneous, synchronous calcium signal was recorded and visualized (Fig. 4b) by using NIH ImageJ by plotting a Z-axis profile for each video and subsequent detection of minimal and maximal calcium signal in the videos and applying color lot to each of them (Fig. 4a). The quantitative graphs indicate regular and spontaneous peaks corresponding to calcium waves (Fig. 4b), revealing no significant differences in the flux frequency as well as intensity and the calcium waves were at a frequency of ~0.5 Hz. These data show that HAGA hydrogels allow appropriate intercellular connections.

3.6. HAGA markedly reduces cell-mediated shrinkage of collagen I hydrogels

Collagen I-based hydrogels provide an excellent matrix for tissue engineering purposes and are widely used, but they have some drawbacks, including shrinkage and cell-induced shrinkage during normal cell culturing time frames [51]. Encapsulated cellular traction onto the collagen I fibrils *in vitro* leads to shrinkage of the tissue engineered construct. We aimed at generating a hydrogel system that resists shrinkage. In order to test whether the here developed hydrogels maintain their size, we resuspended CRL-2429 fibroblasts (2×10^6 cells/mL) directly in the hydrogel precursor, induced gel formation, and maintained them in culture for up to 24 days (Fig. 5). Fibroblasts were chosen as they are important for all tissue types to achieve optimal function [28,52] and as they are known to markedly shrink collagen I hydrogels [53]. Brightfield macroscopic images of the tissues and subsequent quantification of the hydrogel area using NIH ImageJ revealed the stabilizing effect of adding HAGA into the collagen I matrix, evidenced by a shrinkage of <20 % for HAGA60 compared to >90 % shrinkage for collagen I hydrogels within the first 7 days of cell culture (Fig. 5a and b). Long-term experiments revealed that HAGA30 and HAGA60 hydrogels continued to shrink until day 15 (60 % shrinkage) and maintained thereafter their size (Fig. 5b and c). Notably, MWCNTs were not required for shrink resistance, as the shrinkage of HAGA60

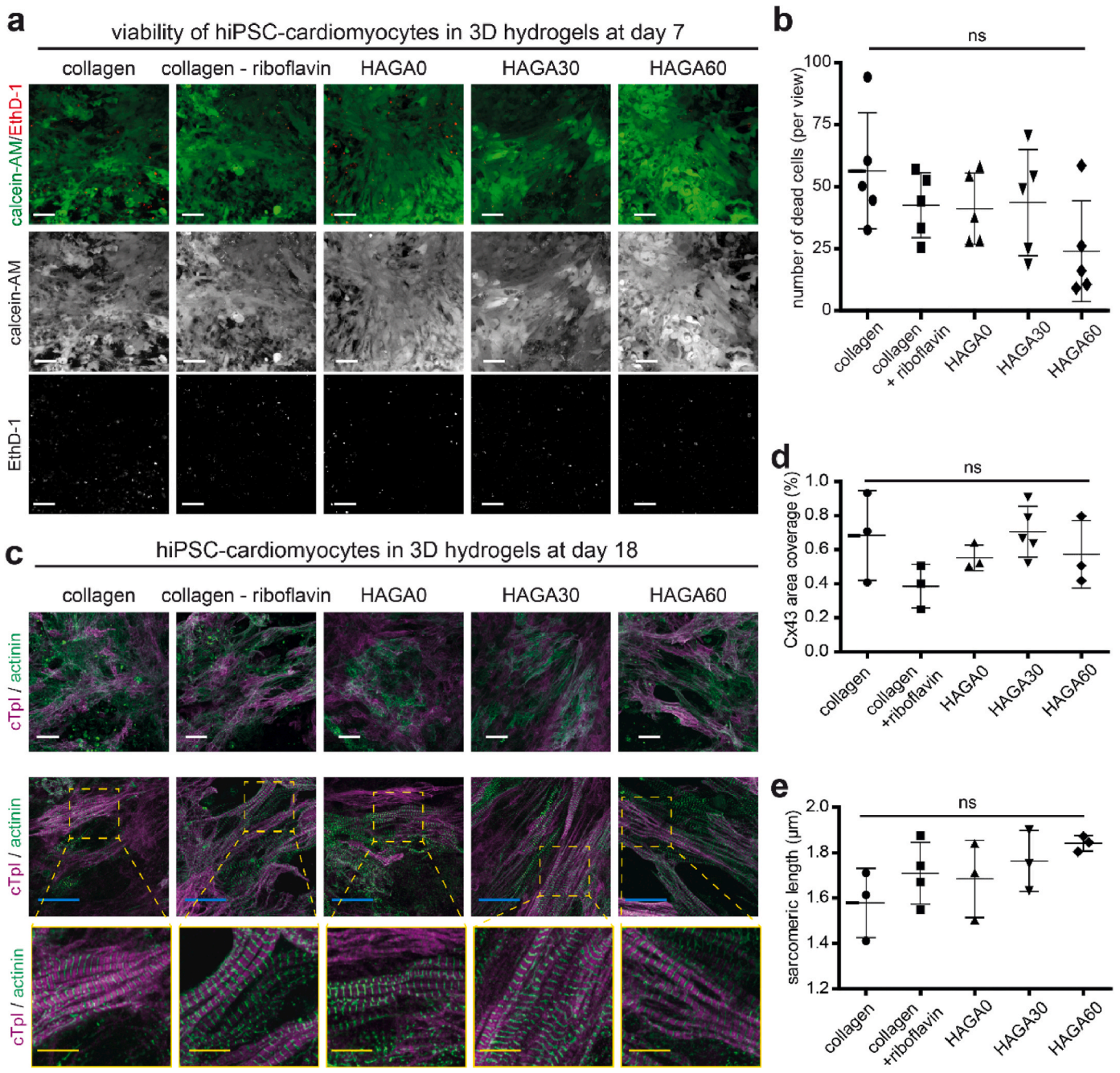

Fig. 3. HAGA hydrogels support the viability and cell spreading of hiPSC-derived cardiomyocytes. (a) Representative images of hiPSC-cardiomyocytes cultured within hydrogels stained with calcein-AM (green, living cells) and EthD-1 (red, dead cells). (b) Quantitative analysis of live and dead staining (n = 3, 3 hiPSC-cardiomyocyte differentiation assays used to generate 5 tissue constructs) based on **a**. (c) Examples projections of confocal images of hiPSC-cardiomyocyte-laden tissue constructs stained for cardiomyocyte-specific markers troponin I and sarcomeric α-actinin (day 18 post-fabrication). DNA was visualized with DAPI. (d) Quantitative analysis of connexin 43 surface coverage (n = 3). (e) Quantitative analysis of sarcomeric length based on confocal images of hiPSC- cardiomyo-cytes stained for troponin I and sarcomeric -actinin. Data is mean ± SD. One-way ANOVA with Bonferroni's posthoc analysis was performed. Scale bars: white: 50 µm, blue: 30 µm, yellow: 10 µm. (For interpretation of the references to color in this figure legend, the reader is referred to the Web version of this article.)

with or without MWCNTs was comparable (Figure S5 a). Taken together, HAGA hydrogels allow the fabrication of tissues with defined size for one week. For long-term experiments, the low shrinkage rate still provides a major advantage over collagen I hydrogels and should allow us to predict size changes.

As shrinkage is mediated by the encapsulated cells, it might be possible that the observed differences in shrinkage between hydrogels are due to different cell numbers caused by different survival or proliferation rates. Live/Dead images of all these tissues after 14 days (Fig. 5d) as well as after 24 days for HAGA30 and HAGA60 with and without MWCNTs (Fig. S5) showed an overall high viability of the cells. To address whether changes in cell number occur over time, mitochondrial activity (Fig. 5e) and DNA content were determined (Fig. 5f). These data show no marked changes in mitochondrial activity or DNA content over time despite obvious shrinkage in collagen I hydrogels in the observed time frames. Taken together, these data exclude the possibility that changes in cell number over time are responsible for the observed shrink-resistant properties of HAGA hydrogels.

To determine, if construct shrinkage changes the mechanical properties, we performed frequency sweep tests on fibroblast-laden

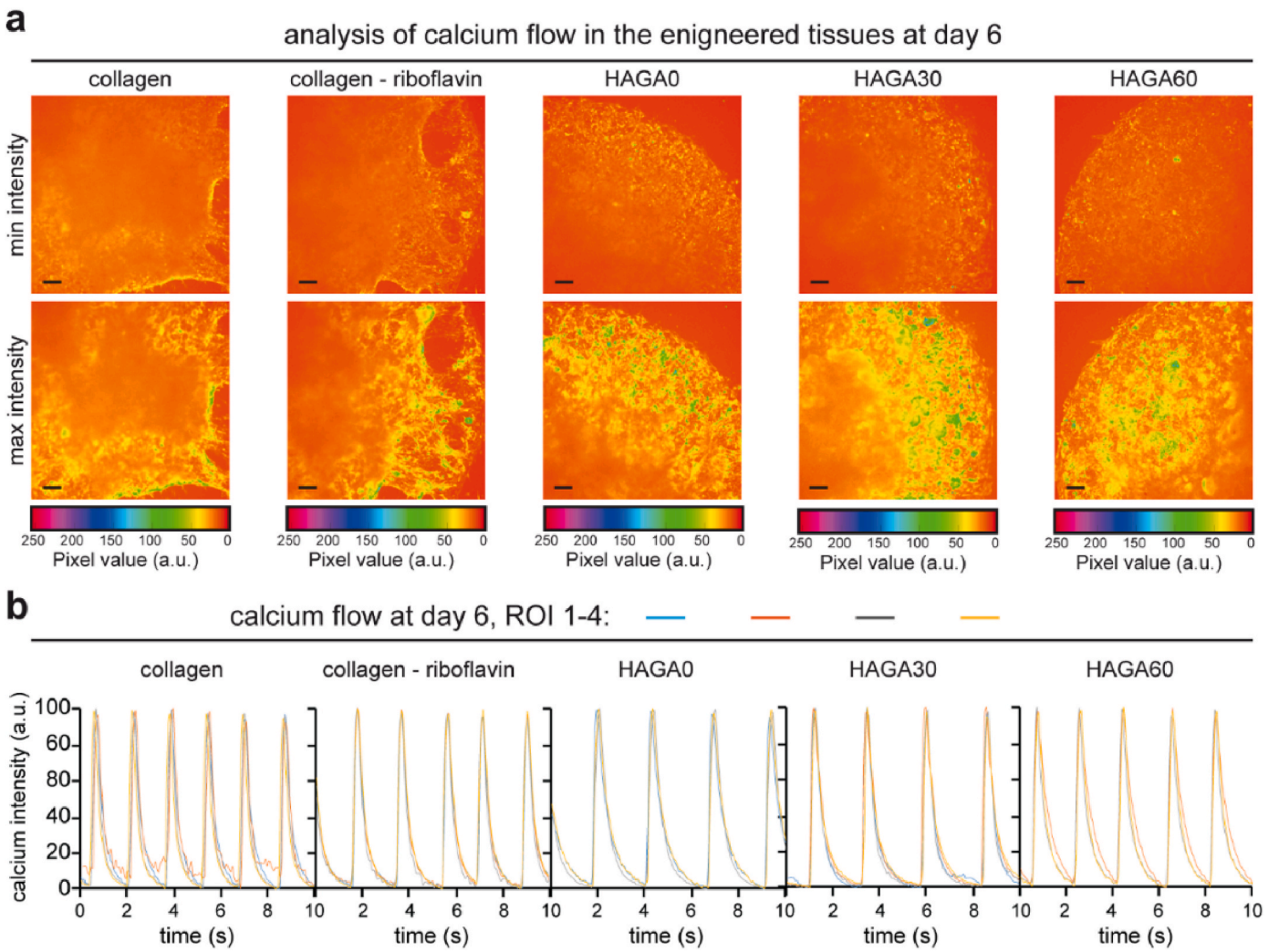

Fig. 4. hiPSC-derived cardiomyocytes show regular pulses of calcium. (a) Local calcium minima and maximum concentration based on Fluo-4 calcium analysis at day 6. (b) Representative examples of intracellular calcium changes in 3D engineered tissues for different ROIs are provided as overlays to indicate synchronous calcium peaks. Scale bar: 200 μm. In **b**, a.u. indicates the arbitrary units.

hydrogels after 3 days in culture to elucidate possible differences in their mechanical properties (Fig. 5g and h). Quantitative analysis of these measurements showed a stabilizing effect of HAGA incorporation into the matrix accompanied by collagen I stiffening in particular compared to HAGA-containing gels in the first three days of culture. In hydrogels containing fibroblasts, the storage modulus (G′) of collagen I hydrogels increased by 6-fold from ~91 Pa at day 0–~566 Pa by day 3. Stiffening also occurred in the collagen-riboflavin group where G′ increased from ~127 Pa at day 0–~284 Pa at day 3. Similarly, G′ increased for HAGA0 group from ~155 Pa on day 0–~432 Pa on day 3. Inclusion of HAGA into the hydrogels in HAGA30 resulted in less stiffening where G′ increased from ~198 Pa at day 0–~296 Pa at day 3. Conversely, we noticed a slight softening in HAGA60 where G' decreased from ~378 Pa to ~349 Pa over the course of three days. Notably, such shrink resitive hydrogels allowed proper cardiomyocyte function (Fig. 4) as well as fibroblast spreading and growth while maintaining the geometry (Figs. 5 and 6).

3.7. HAGA60 is an ink suitable for 3D bioprinting

The shrink-resistant characteristic of HAGA60 is unique and makes it a good candidate as ink for 3D bioprinting. Therefore, we have evaluated the rheological properties, 3D bioprinting capability, and cellular compatibility of HAGA60 (Fig. 6).

We assessed the shear-thinning characteristic of HAGA60 utilizing rheological analysis. Quantitative analysis of viscosity over a range of shear rates from 0.01 to 10 Hz showed a high viscosity of HAGA60 at low shear rates, which was inversely correlated with increasing the shear rates, confirming shear-thinning properties, which are critical for extrusion-based 3D bioprinting (Fig. 6a). The shear-thinning behavior of HAGA60 was similar at 10 °C or 37 °C whether or not being crosslinked by blue light. These data show that HAGA60 is extrudable at different temperatures. Moreover, we found that exposure to the blue light triggered an immediate increase in storage modulus (G′) and its dominance over the loss modulus (G″), indicating network formation and a more solid-like behavior of the ink. This sharp increase in G' upon blue light exposure indicates successful photo-crosslinking. Modeling the rheological behavior of HAGA60 based on Herschel-Bulkley Model Fit, demonstrated its yield stress (~0.55 Pa) and shear-thinning behavior ($\tau = \tau_0 + k \cdot \gamma^n$) with a strong model fit ($R^2 = 0.9928$) suggesting a reliable characterization (Fig. 6c). Thixotropic recovery is crucial for extrusion-based bioprinting, thus, we measured this characteristic of HAGA60 by subjecting it to alternating low and high shear rates (Fig. 6d). This data confirmed that HAGA60 consistently recovers its viscosity after each high-shear event, indicating excellent thixotropic behavior. However, it is noteworthy that the yield stress of HAGA60 is relatively low, which could make the printed constructs susceptible to deformation. This necessitates the use of either higher solid content, or additional stabilizers

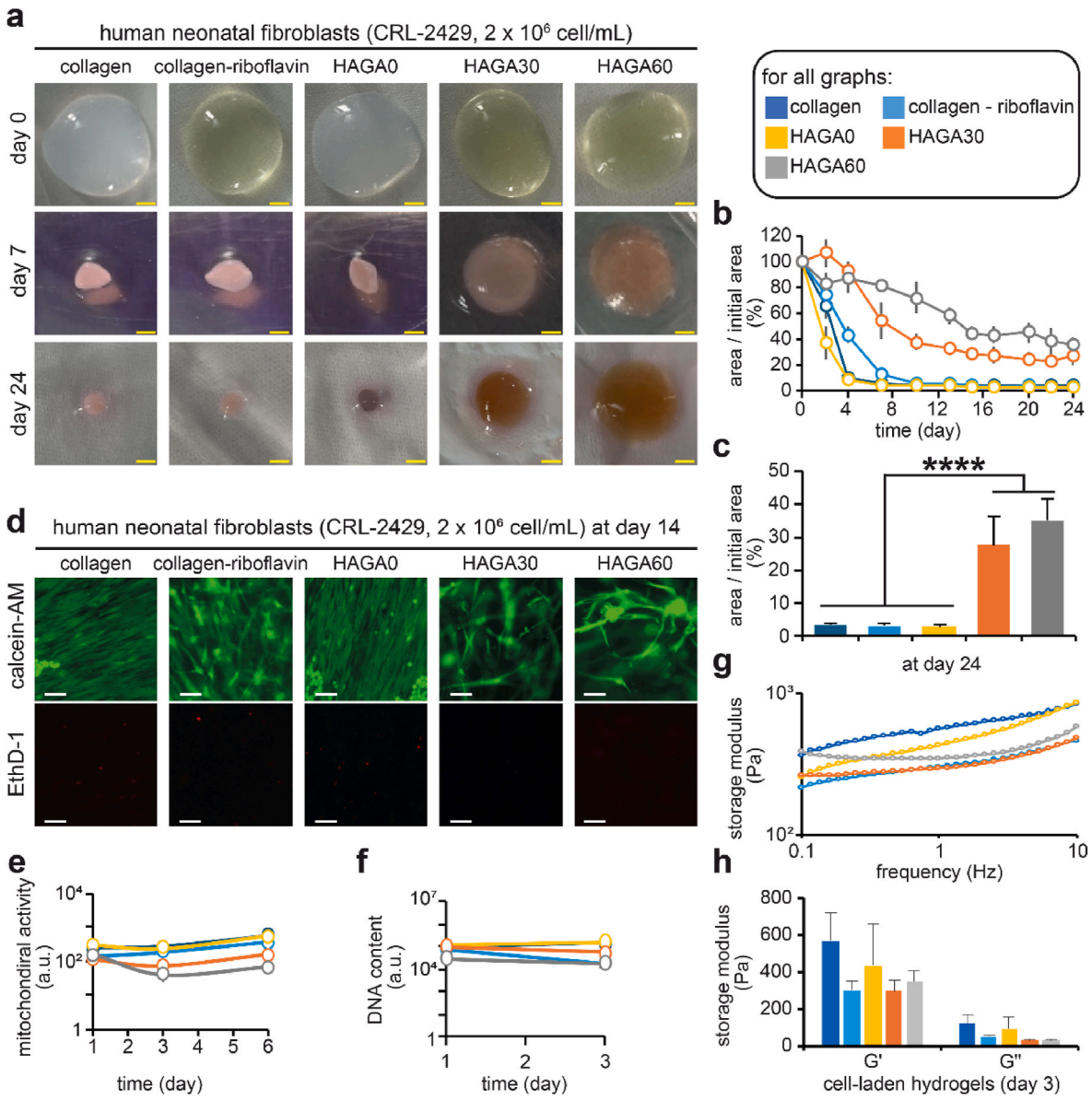

Fig. 5. Gallic acid-functionalized hyaluronic acid maintains geometry of collagen I hydrogels. (a) Representative photographs of cell-laden hydrogels on day 0, day 7, and day 24. (b) Quantified shrinkage of hydrogels over time for 24 days (n = 3). (c) Shrinkage of cell-laden hydrogels on day 24. (d) Representative epi-fluorescent microscopy images of CRL-2429 fibroblasts in 3D hydrogels at day 14. (e) Quantitative analysis of mitochondrial activity of cells in the bulk of hydrogels based on Presto blue assay (n = 3). (f) Quantitative analysis of the DNA content in each hydrogel group over 3 days based on Cyquant assay kit (n = 3). (g) Evaluation of storage modulus of cell-laden hydrogels at day 3 based on frequency sweep test. (h) Storage G′ and loss modulus G″ of cell-laden hydrogels on day 3. Data is mean ± SD. Scale bars: white: 50 μm, yellow: 2.2 mm. (For interpretation of the references to color in this figure legend, the reader is referred to the Web version of this article.)

to enhance the structural integrity post-printing. Therefore, we designed an approach to 3D bioprint this material in a support bath of gelatin microparticles. As a proof of concept, we have resuspended human neonatal CRL-2429 fibroblasts at 1 and 2 × 10^6 cells/mL ink and 3D-bioprinted rings. We have prepared a support bath of gelatin/gum arabic, as reported previously [27]. This support bath exhibits self-healing properties and provides a supportive environment for 3D bioprinting of soft hydrogels. To assess the printability of HAGA60 hydrogel in the above-described support bath, a 3D design of a ring with a diameter of 10 mm, height of 1 mm, and filament thickness of 0.1 mm was generated in license-free Autodesk Tinkercad platform, and the stl file was imported in an Allevi 3 bioprinter to print the tissues. Cell-laden hydrogel precursor was loaded into a 5 mL syringe which was then inserted into the printer. The rings were 3D-bioprinted into the support bath and exposed to blue light (90 % intensity, 5 min). Subsequently, the rings inside the support bath were placed in an incubator at 37 °C and 5 % CO_2 for 30 min to melt the support bath and extract the 3D-bioprinted rings (Fig. 6e).

We have monitored the 3D-bioprinted rings for up to 7 days to assess whether shrinkage of the rings due to the presence of fibroblasts occurs (Fig. 6f). The stereomicroscopic images of the bioprinted rings at 1 and 7 days post-printing showed almost no shrinkage of the 3D-bioprinted rings (Fig. 6f). When HAGA60, which forms a soft gel, was printed into the support bath with a low cell density of 1 × 10^6 cells/mL, we observed a deformity in the circular shape of the 3D-bioprinted rings. However, by increasing the cell density to 2 × 10^6 cells/mL, the 3D-bioprinted constructs remained circular throughout the 7 days observation. In order to evaluate the behavior of fibroblasts within the 3D-bioprinted rings, we performed immunostaining analysis after 7 days in culture. The confocal laser scanning microscopic images showed fibroblasts

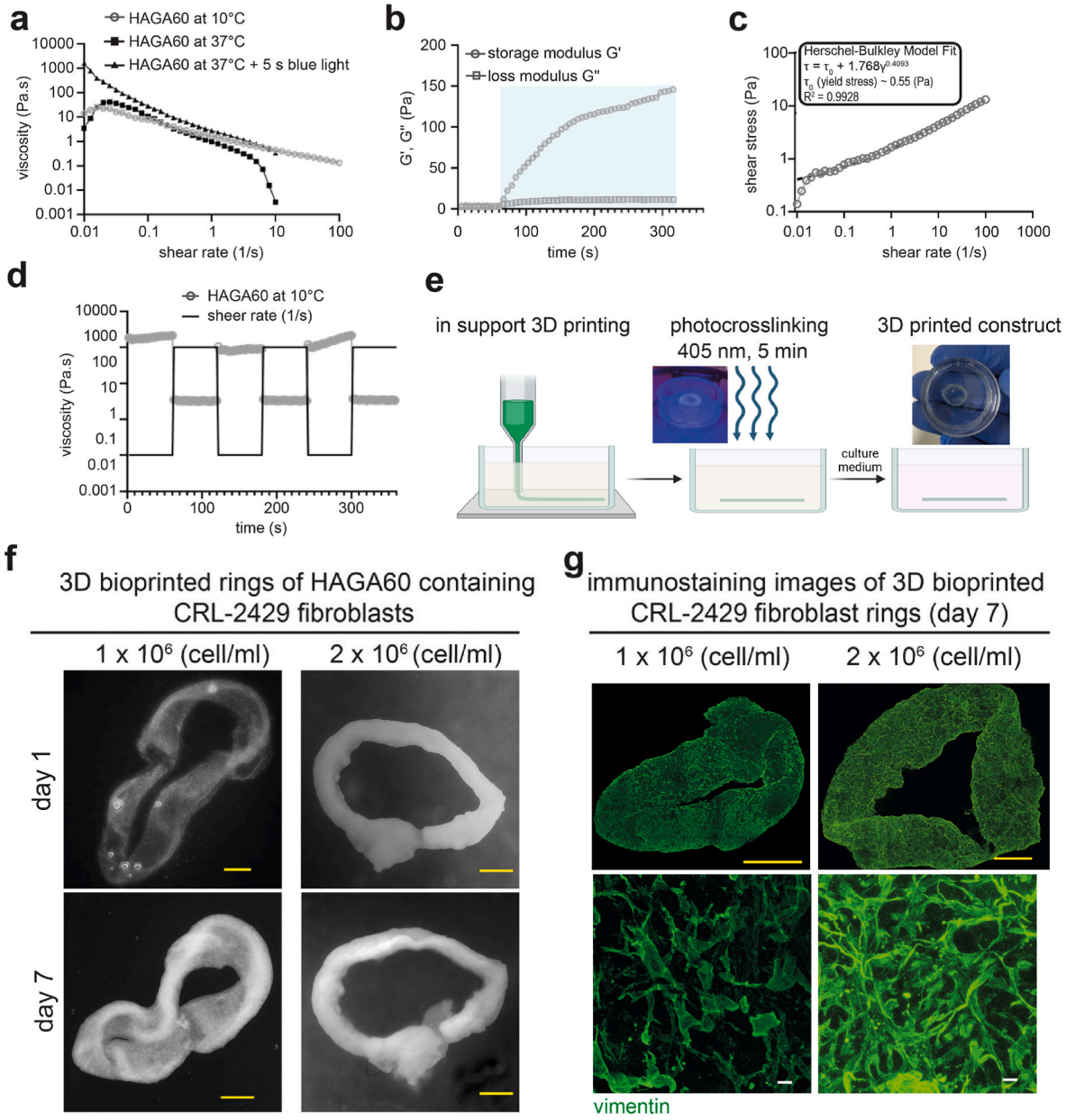

Fig. 6. Rheological characterization, 3D bioprinting, and cellular compatibility of HAGA60 bioink. (a) Viscosity of HAGA60 as a function of shear rate at 10 °C, 37 °C, and 37 °C with blue light exposure. (b) Storage modulus (G′) and loss modulus (G″) of HAGA60 over time at 37 °C during blue light photo-crosslinking (405 nm, 5 min). (c) Shear stress vs. shear rate curve of HAGA60 fitted to the Herschel-Bulkley model ($\tau = \tau_0 + k \cdot \gamma^n$), showing a yield stress of 0.55 Pa and strong shear-thinning behavior ($R^2 = 0.9928$). (d) Thixotropic recovery of HAGA60 during alternating low and high shear rate cycles. (e) Schematic representation of 3D bioprinting procedure. (f) Representative stereoscopic images of 3D-bioprinted rings at day 1 and 7. (g) Examples of projections of confocal images of CRL-2429-laden 3D-bioprinted HAGA60 stained for vimentin and nuclei by DAPI (day 7 after printing). Scale bars: yellow: 1000 μm, white: 20 μm. (For interpretation of the references to color in this figure legend, the reader is referred to the Web version of this article.)

spreading, extending, and forming an interconnected cellular network at both cell densities (Fig. 6g). As expected, when the shape is maintained, the compactness of the cellular network increased with the number of cells loaded in the bioink. Taken together, these data show that HAGA60 is shrink-resistant, 3D-bioprintable, and cytocompatible.

The suitability of HAGA60 and its support for fibroblasts convinced us to further evaluate this bioink for more complex systems. Hence, we 3D-bioprinted different geometric models of cardiac ventricles based on hiPSC-cardiomyocyte-laden HAGA60 in a support bath of gelatin microparticles (Fig. 7).

We designed two stl files of ventricle shapes with different opening diameters. The ventricles were 5 mm × 5 mm x 5.21 mm (X:Y:Z) for the smaller opening and 5 mm × 5 mm x 4 mm (X:Y:Z) for the bigger opening. Stereomicroscopic images of 3D-bioprinted ventricles after 20 days showed that the opening of both models remained open, suggesting successful preservation of the lumen in the 3D-bioprinted constructs (Fig. 7a). We have evaluated the shrinkage of the 3D-bioprinted ventricles over 30 days in culture. HAGA60-bioprinted ventricles maintained their size and shape up to 5 days and compacted to ~75 % after 8 days. The compaction continued until day 12, reaching a plateau at ~40 % of their initial size, still maintaining a ventricle-like shape (Fig. 7b and c). The culture media for these ventricles were changed every 2 days and the bioprinted constructs started to beat after 7–10 days and maintained their contraction throughout the experimental period (Movie S2). We evaluated the responsiveness of the 3D-bioprinted ventricles to pharmacological stimulation with epinephrine (50 μM), which is known to

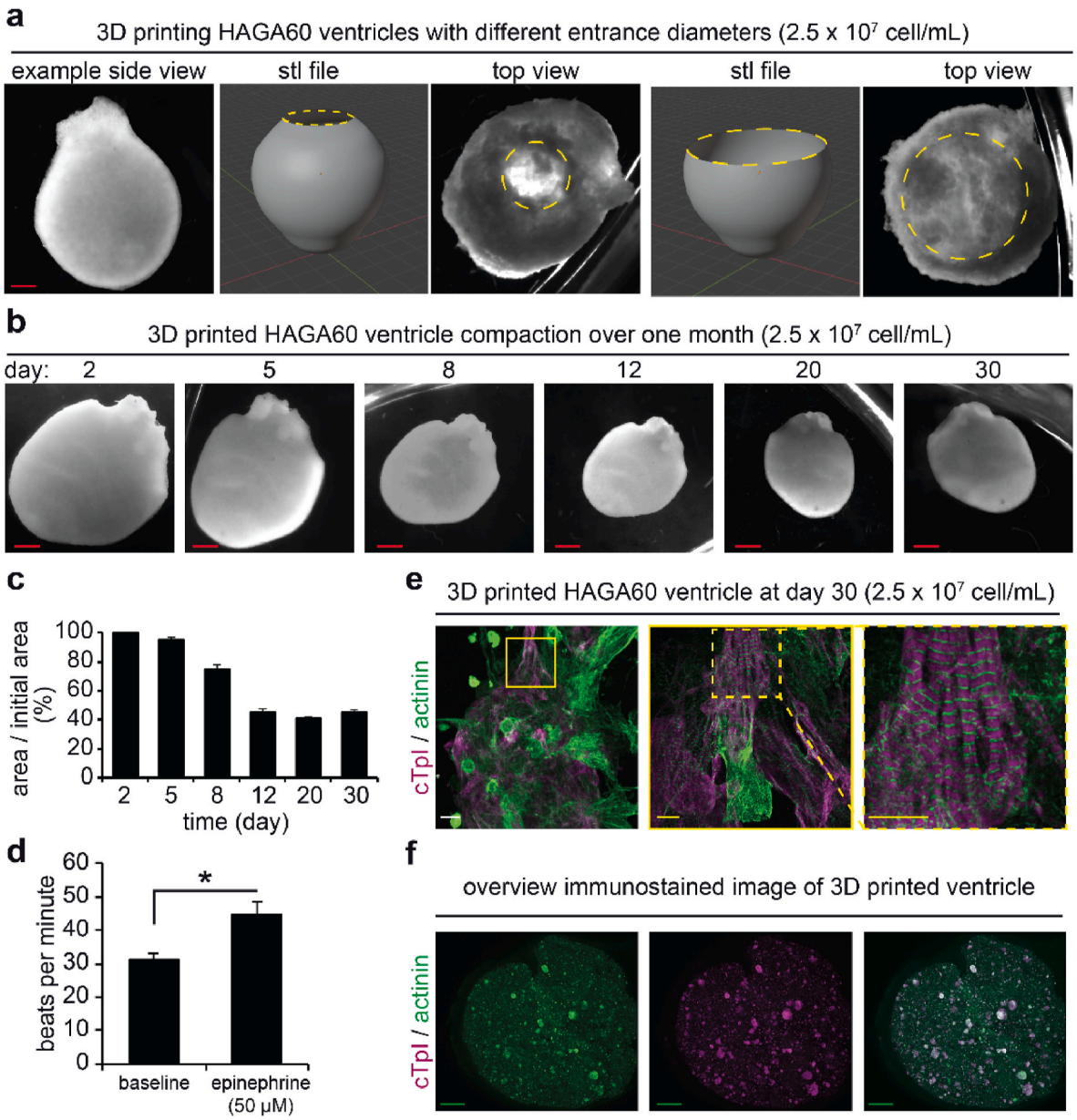

Fig. 7. 3D bioprinting HAGA60 ventricles containing hiPSC-cardiomyocytes. (a) 3D-bioprinted HAGA60 ventricle-shaped constructs loaded with 2.5 × 10^7 cells/mL. Side and top view images of the printed constructs and their respective STL files, illustrating varying opening diameters (dashed yellow circles). (b) Time-lapse brightfield microscopy images showing compaction of 3D-bioprinted ventricles over 30 days in culture. (c) Quantification of construct compaction, represented as the percentage of the initial area over time (n = 3). (d) Functional assessment of bioprinted ventricles at day 30, showing increased contraction frequency upon exposure to epinephrine (50 µM). (e) High-resolution immunostaining of the 3D-bioprinted ventricle at day 30, showing cardiac troponin I (cTnI, magenta) and α-actinin (green). The boxed regions show sarcomere organization at increasing magnifications, confirming cardiomyocyte differentiation. (f) Overview images of an immunostained 3D-bioprinted ventricle at day 30, showing cTnI (magenta) and α-actinin (green) distribution throughout the construct, indicating uniform cardiomyocyte integration and differentiation. Data are presented as mean ± SD, *: $p < 0.05$. Scale bars: red: 1 mm, white: 20 µm, yellow: 10 µm, green: 500 µm. (For interpretation of the references to color in this figure legend, the reader is referred to the Web version of this article.)

enhance cardiomyocyte beating rates [27,31,34]. The bioprinted ventricles significantly increased their beating rate directly upon stimulation (Fig. 7d and Movie S3). A closer analysis of the cellular contractile machinery by immunostaining against cardiac troponin I (cTp I) and sarcomeric alpha-actinin (actinin) revealed that cardiomyocytes within bioprinted HAGA60 established and maintained well-striated sarcomeres, indicating proper subcellular organization of the contractile machinery in these cardiomyocytes (Fig. 7e). Notably, an overview laser confocal microscopic image of the bioprinted ventricle showed that cTpI, a marker of more mature cardiomyocytes, is broadly expressed within the ventricle (Fig. 7f).

4. Conclusion

Collectively, we have developed a hydrogel system based on ECM polymers that is resistant against cell-mediated hydrogel shrinkage, is cytocompatible, and allows 3D bioprinting of cell-laden constructs. Several lines of evidence support our conclusions. First, hiPSC-cardiomyocytes and human fibroblasts exhibited normal cell behavior and/or function in this hydrogel system. Second, fibroblast-laden HAGA60-hydrogels, whether casted or printed, shrink markedly less compared to collagen I hydrogels. Interestingly, this hydrogel is tissue adhesive and exhibits radical scavenging properties. The here developed hydrogels exhibited enhanced mechanical stiffness owing to the

chemistry that has been used in the generation protocol offering a versatile platform for generating engineered cardiac tissues.

CRediT authorship contribution statement

Kaveh Roshanbinfar: Writing – review & editing, Writing – original draft, Validation, Software, Project administration, Methodology, Investigation, Formal analysis, Data curation. **Austin Donnelly Evans:** Writing – review & editing, Writing – original draft, Visualization, Validation, Methodology, Investigation, Formal analysis, Data curation. **Sumanta Samanta:** Writing – original draft, Methodology, Formal analysis, Conceptualization. **Maria Kolesnik-Gray:** Writing – original draft, Validation, Formal analysis, Data curation. **Maren Fiedler:** Data curation. **Vojislav Krstic:** Writing – original draft, Supervision, Funding acquisition, Formal analysis, Data curation. **Felix B. Engel:** Writing – review & editing, Supervision, Resources, Methodology, Investigation, Funding acquisition, Data curation, Conceptualization. **Oommen P. Oommen:** Writing – review & editing, Writing – original draft, Supervision, Resources, Investigation, Funding acquisition, Formal analysis, Conceptualization.

Declaration of competing interest

The authors declare that they have no known competing financial interests or personal relationships that could have appeared to influence the work reported in this paper.

Acknowledgments

This research was funded by Universitätsklinikum Erlangen ELAN IZKF, grant number P093/Aktenzeichen: 21-05-20-1-Roshanbinfar, the Deutsche Forschungsgemeinschaft [DFG, German Research Foundation, grant numbers: Projektnummer 326998133 – TRR 225 (seed fund to KR, subproject C01 to F.B.E.) and INST 410/91-1 FUGG to F.B.E.), the Deutsche Herzstiftung e.V. (to F.B.E.), the Manfred Roth Stiftung (to F.B.E.), the Research Foundation Medicine at the University Clinic Erlangen, Germany (to F.B.E.), the Sigrid Juselius Foundation, project number 230140 (to OPO), Syöpäsäätiö, # 240150 Cancer Foundation Finland (to OPO), Linnea Pirilä Fund from the Finnish Cultural Foundation Pirkanmaa Regional Fund Grant #50241473, and Tampere University Doctoral School Fund (to ADE). Graphical illustrations have been generated by BioRender and ChemBioDraw. We would further like to acknowledge Aybike Kocatürkmen for helping with the DPPH scavenging assay.

Appendix A. Supplementary data

Supplementary data to this article can be found online at https://doi.org/10.1016/j.biomaterials.2025.123174.

Data availability

Data will be made available on request.

References

[1] J. Groll, T. Boland, T. Blunk, J.A. Burdick, D.W. Cho, P.D. Dalton, B. Derby, G. Forgacs, Q. Li, V.A. Mironov, L. Moroni, M. Nakamura, W. Shu, S. Takeuchi, G. Vozzi, T.B. Woodfield, T. Xu, J.J. Yoo, J. Malda, Biofabrication: reappraising the definition of an evolving field, Biofabrication 8 (1) (2016) 013001.

[2] N. Gjorevski, M. Nikolaev, T.E. Brown, O. Mitrofanova, N. Brandenberg, F. W. DelRio, F.M. Yavitt, P. Liberali, K.S. Anseth, M.P. Lutolf, Tissue geometry drives deterministic organoid patterning, Science 375 (6576) (2022) eaaw9021.

[3] R. Levato, T. Jungst, R.G. Scheuring, T. Blunk, J. Groll, J. Malda, From shape to function: the next step in bioprinting, Adv. Mater. 32 (12) (2020) e1906423.

[4] I.N. Amirrah, Y. Lokanathan, I. Zulkiflee, M. Wee, A. Motta, M.B. Fauzi, A comprehensive review on collagen type I development of biomaterials for tissue engineering: from biosynthesis to bioscaffold, Biomedicines 10 (9) (2022).

[5] M. Shahbazi, H. Jager, Current status in the utilization of biobased polymers for 3D printing process: a systematic review of the materials, processes, and challenges, ACS Appl. Bio Mater. 4 (1) (2021) 325–369.

[6] Y. Wang, Z. Wang, Y. Dong, Collagen-based biomaterials for tissue engineering, ACS Biomater. Sci. Eng. 9 (3) (2023) 1132–1150.

[7] M. Zheng, X. Wang, Y. Chen, O. Yue, Z. Bai, B. Cui, H. Jiang, X. Liu, A review of recent progress on collagen-based biomaterials, Adv. Healthcare Mater. 12 (16) (2023) e2202042.

[8] J. Jokinen, E. Dadu, P. Nykvist, J. Kapyla, D.J. White, J. Ivaska, P. Vehvilainen, H. Reunanen, H. Larjava, L. Hakkinen, J. Heino, Integrin-mediated cell adhesion to type I collagen fibrils, J. Biol. Chem. 279 (30) (2004) 31956–31963.

[9] M. Leiss, K. Beckmann, A. Giros, M. Costell, R. Fassler, The role of integrin binding sites in fibronectin matrix assembly in vivo, Curr. Opin. Cell Biol. 20 (5) (2008) 502–507.

[10] C. Patra, F. Diehl, F. Ferrazzi, M.J. van Amerongen, T. Novoyatleva, L. Schaefer, C. Muhlfeld, B. Jungblut, F.B. Engel, Nephronectin regulates atrioventricular canal differentiation via Bmp4-Has2 signaling in zebrafish, Development 138 (20) (2011) 4499–4509.

[11] C. Patra, F. Ricciardi, F.B. Engel, The functional properties of nephronectin: an adhesion molecule for cardiac tissue engineering, Biomaterials 33 (17) (2012) 4327–4335.

[12] M. Ahearne, Introduction to cell-hydrogel mechanosensing, Interface Focus 4 (2) (2014) 20130038.

[13] M.A. Schwartz, Integrins and extracellular matrix in mechanotransduction, Cold Spring Harb Perspect Biol 2 (12) (2010) a005066.

[14] F.J. Vernerey, S. Lalitha Sridhar, A. Muralidharan, S.J. Bryant, Mechanics of 3D cell-hydrogel interactions: experiments, models, and mechanisms, Chem Rev 121 (18) (2021) 11085–11148.

[15] Y.K. Zhu, T. Umino, X.D. Liu, H.J. Wang, D.J. Romberger, J.R. Spurzem, S. I. Rennard, Contraction of fibroblast-containing collagen gels: initial collagen concentration regulates the degree of contraction and cell survival, In Vitro Cell. Dev. Biol. Anim. 37 (1) (2001) 10–16.

[16] G.N. Iaconisi, P. Lunetti, N. Gallo, A.R. Cappello, G. Fiermonte, V. Dolce, L. Capobianco, Hyaluronic acid: a powerful biomolecule with wide-ranging applications-A comprehensive review, Int. J. Mol. Sci. 24 (12) (2023).

[17] S. Samanta, V.K. Rangasami, N.A. Murugan, V.S. Parihar, O.P. Varghese, O. P. Oommen, An unexpected role of an extra phenolic hydroxyl on the chemical reactivity and bioactivity of catechol or gallol modified hyaluronic acid hydrogels, Polym Chem-Uk 12 (20) (2021) 2987–2991.

[18] S. Samanta, L. Yla-Outinen, V.K. Rangasami, S. Narkilahti, O.P. Oommen, Bidirectional cell-matrix interaction dictates neuronal network formation in a brain-mimetic 3D scaffold, Acta Biomater. 140 (2022) 314–323.

[19] S. Samanta, V.K. Rangasami, H. Sarlus, J.R.K. Samal, A.D. Evans, V.S. Parihar, O. P. Varghese, R.A. Harris, O.P. Oommen, Interpenetrating gallol functionalized tissue adhesive hyaluronic acid hydrogel polarizes macrophages to an immunosuppressive phenotype, Acta Biomater. 142 (2022) 36–48.

[20] S.H. Liu, A. Bernhardt, K. Wirsig, A. Lode, Q.X. Hu, M. Gelinsky, D. Kilian, Synergy of Inorganic and Organic Inks in Bioprinted Tissue Substitutes: Construct Stability and Cell Response during Long-Term Cultivation, vol. 261, Compos Part B-Eng, 2023.

[21] E. Silberman, H. Oved, M. Namestnikov, A. Shapira, T. Dvir, Post-maturation reinforcement of 3D-printed vascularized cardiac tissues, Adv. Mater. 35 (31) (2023) e2302229.

[22] H. Chen, F. Fei, X. Li, Z. Nie, D. Zhou, L. Liu, J. Zhang, H. Zhang, Z. Fei, T. Xu, A facile, versatile hydrogel bioink for 3D bioprinting benefits long-term subaqueous fidelity, cell viability and proliferation, Regen Biomater 8 (3) (2021) rbab026.

[23] M. Proestaki, M. Sarkar, B.M. Burkel, S.M. Ponik, J. Notbohm, Effect of hyaluronic acid on microscale deformations of collagen gels, J. Mech. Behav. Biomed. Mater. 135 (2022) 105465.

[24] J. Gong, C.C.L. Schuurmans, A.M.V. Genderen, X. Cao, W. Li, F. Cheng, J.J. He, A. Lopez, V. Huerta, J. Manriquez, R. Li, H. Li, C. Delavaux, S. Sebastian, P. E. Capendale, H. Wang, J. Xie, M. Yu, R. Masereeuw, T. Vermonden, Y.S. Zhang, Complexation-induced resolution enhancement of 3D-printed hydrogel constructs, Nat. Commun. 11 (1) (2020) 1267.

[25] L.G. Brunel, F. Christakopoulos, D. Kilian, B. Cai, S.M. Hull, D. Myung, S. C. Heilshorn, Embedded 3D bioprinting of collagen inks into microgel baths to control hydrogel microstructure and cell spreading, Adv. Healthcare Mater. (2023) e2303325.

[26] A. Moro, S. Samanta, L. Honkamaki, V.K. Rangasami, P. Puistola, M. Kauppila, S. Narkilahti, S. Miettinen, O. Oommen, H. Skottman, Hyaluronic acid based next generation bioink for 3D bioprinting of human stem cell derived corneal stromal model with innervation, Biofabrication 15 (1) (2022).

[27] T.U. Esser, A. Anspach, K.A. Muenzebrock, D. Kah, S. Schrufer, J. Schenk, K. G. Heinze, D.W. Schubert, B. Fabry, F.B. Engel, Direct 3D-bioprinting of hiPSC-derived cardiomyocytes to generate functional cardiac tissues, Adv. Mater. 35 (52) (2023) e2305911.

[28] M. Tiburcy, J.E. Hudson, P. Balfanz, S. Schlick, T. Meyer, M.L. Chang Liao, E. Levent, F. Raad, S. Zeidler, E. Wingender, J. Riegler, M. Wang, J.D. Gold, I. Kehat, E. Wettwer, U. Ravens, P. Dierickx, L.W. van Laake, M.J. Goumans, S. Khadjeh, K. Toischer, G. Hasenfuss, L.A. Couture, A. Unger, W.A. Linke, T. Araki, B. Neel, G. Keller, L. Gepstein, J.C. Wu, W.H. Zimmermann, Defined engineered human myocardium with advanced maturation for applications in heart failure modeling and repair, Circulation 135 (19) (2017) 1832–1847.

[29] K. Roshanbinfar, J. Hilborn, O.P. Varghese, O.P. Oommen, Injectable and thermoresponsive pericardial matrix derived conductive scaffold for cardiac tissue engineering, Rsc Adv 7 (51) (2017) 31980–31988.
[30] K. Roshanbinfar, Z. Mohammadi, A.S.M. Mesgar, M.M. Dehghan, O.P. Oommen, J. Hilborn, F.B. Engel, Carbon nanotube doped pericardial matrix derived electroconductive biohybrid hydrogel for cardiac tissue engineering, Biomater Sci-Uk 7 (9) (2019) 3906–3917.
[31] K. Roshanbinfar, M. Schiffer, E. Carls, M. Angeloni, M. Kolesnik-Gray, S. Schruefer, D.W. Schubert, F. Ferrazzi, V. Krstic, B.K. Fleischmann, W. Roell, F.B. Engel, Electrically conductive collagen-PEDOT:PSS hydrogel prevents post-infarct cardiac arrhythmia and supports hiPSC-cardiomyocyte function, Adv. Mater. (2024) 2403642.
[32] D.K. Schroder, Semiconductor Material and Device Characterization, John Wiley & Sons, Ltd., New York2005.
[33] J.Y. Lai, L.J. Luo, Antioxidant gallic acid-functionalized biodegradable in situ gelling copolymers for cytoprotective antiglaucoma drug delivery systems, Biomacromolecules 16 (9) (2015) 2950–2963.
[34] K. Roshanbinfar, L. Vogt, B. Greber, S. Diecke, A.R. Boccaccini, T. Scheibel, F. B. Engel, Electroconductive biohybrid hydrogel for enhanced maturation and beating properties of engineered cardiac tissues, Adv. Funct. Mater. 28 (42) (2018) 1803951.
[35] K. Roshanbinfar, M.K. Gray, S. Schruefer, D.W. Schubert, V. Krstic, F.B. Engel, Polyethyleneimine-decorated gold nanoparticles for simultaneous drug release and enhanced beating properties of hiPSC-derived cardiomyocytes in 3D engineered cardiac tissues, Tissue Eng Pt A 29 (13–14) (2023).
[36] K. Roshanbinfar, M. Kolesnik-Gray, M. Angeloni, S. Schruefer, M. Fiedler, D. W. Schubert, F. Ferrazzi, V. Krstic, F.B. Engel, Collagen hydrogel containing polyethylenimine-gold nanoparticles for drug release and enhanced beating properties of engineered cardiac tissues, Adv. Healthcare Mater. 12 (20) (2023) 2202408.
[37] K. Roshanbinfar, L. Vogt, F. Ruther, J.A. Roether, A.R. Boccaccini, F.B. Engel, Nanofibrous composite with tailorable electrical and mechanical properties for cardiac tissue engineering, Adv. Funct. Mater. 30 (7) (2020) 1908612.
[38] R.A. MacDonald, C.M. Voge, M. Kariolis, J.P. Stegemann, Carbon nanotubes increase the electrical conductivity of fibroblast-seeded collagen hydrogels, Acta Biomater. 4 (6) (2008) 1583–1592.
[39] M.S. Dopico-García, A. Ares, A. Lasagabáster-Latorre, X. García, L. Arboleda, M. J. Abad, Extruded polyaniline/EVA blends: enhancing electrical conductivity using gallate compatibilizers, Synthetic Met 189 (2014) 193–202.
[40] U. Blache, E.M. Ford, B. Ha, L. Rijns, O. Chaudhuri, P.Y.W. Dankers, A.M. Kloxin, J. G. Snedeker, E. Gentleman, Engineered hydrogels for mechanobiology, Nat Rev Methods Primers 2 (2022) 98.
[41] S.F. Schlick, F. Spreckelsen, M. Tiburcy, L.M. Iyer, T. Meyer, L.C. Zelarayan, S. Luther, U. Parlitz, W.H. Zimmermann, F. Rehfeldt, Agonistic and antagonistic roles of fibroblasts and cardiomyocytes on viscoelastic stiffening of engineered human myocardium, Prog. Biophys. Mol. Biol. 144 (2019) 51–60.
[42] P.A. Wassenaar, C.N. Eleswarpu, S.A. Schroeder, X. Mo, B.D. Raterman, R. D. White, A. Kolipaka, Measuring age-dependent myocardial stiffness across the cardiac cycle using MR elastography: a reproducibility study, Magn. Reson. Med. 75 (4) (2016) 1586–1593.
[43] F.F. Fontenele, N. Bouklas, Understanding the inelastic response of collagen fibrils: a viscoelastic-plastic constitutive model, Acta Biomater. 163 (2023) 78–90.
[44] O.P. Oommen, S.J. Wang, M. Kisiel, M. Sloff, J. Hilborn, O.P. Varghese, Smart design of stable extracellular matrix mimetic hydrogel: Synthesis, characterization, and in vitro and in vivo evaluation for tissue engineering, Adv. Funct. Mater. 23 (10) (2013) 1273–1280.
[45] G.A. Roth, G.A. Mensah, C.O. Johnson, G. Addolorato, E. Ammirati, L.M. Baddour, N.C. Barengo, A.Z. Beaton, E.J. Benjamin, C.P. Benziger, A. Bonny, M. Brauer, M. Brodmann, T.J. Cahill, J. Carapetis, A.L. Catapano, S.S. Chugh, L.T. Cooper, J. Coresh, M. Criqui, N. DeCleene, K.A. Eagle, S. Emmons-Bell, V.L. Feigin, J. Fernandez-Sola, G. Fowkes, E. Gakidou, S.M. Grundy, F.J. He, G. Howard, F. Hu, L. Inker, G. Karthikeyan, N. Kassebaum, W. Koroshetz, C. Lavie, D. Lloyd-Jones, H. S. Lu, A. Mirijello, A.M. Temesgen, A. Mokdad, A.E. Moran, P. Muntner, J. Narula, B. Neal, M. Ntsekhe, G. Moraes de Oliveira, C. Otto, M. Owolabi, M. Pratt, S. Rajagopalan, M. Reitsma, A.L.P. Ribeiro, N. Rigotti, A. Rodgers, C. Sable, S. Shakil, K. Sliwa-Hahnle, B. Stark, J. Sundstrom, P. Timpel, I.M. Tleyjeh, M. Valgimigli, T. Vos, P.K. Whelton, M. Yacoub, L. Zuhlke, C. Murray, V. Fuster, GGBD-NHLBI-JACC Global Burden of Cardiovascular Diseases Writing Group Group, Global burden of cardiovascular diseases and risk factors, 1990-2019: update from the GBD 2019 study, J. Am. Coll. Cardiol. 76 (25) (2020) 2982–3021.
[46] P.L. Bernier, A. Stefanescu, G. Samoukovic, C.I. Tchervenkov, The challenge of congenital heart disease worldwide: epidemiologic and demographic facts, Semin. Thorac. Cardiovasc. Surg. Pediatr. Card. Surg. Annu. 13 (1) (2010) 26–34.
[47] L. Gao, M.E. Kupfer, J.P. Jung, L. Yang, P. Zhang, Y. Da Sie, Q. Tran, V. Ajeti, B. T. Freeman, V.G. Fast, P.J. Campagnola, B.M. Ogle, J. Zhang, Myocardial tissue engineering with cells derived from human-induced pluripotent stem cells and a native-like, high-resolution, 3-dimensionally printed scaffold, Circ. Res. 120 (8) (2017) 1318–1325.
[48] M. Kawamura, S. Miyagawa, K. Miki, A. Saito, S. Fukushima, T. Higuchi, T. Kawamura, T. Kuratani, T. Daimon, T. Shimizu, T. Okano, Y. Sawa, Feasibility, safety, and therapeutic efficacy of human induced pluripotent stem cell-derived cardiomyocyte sheets in a porcine ischemic cardiomyopathy model, Circulation 126 (11 Suppl 1) (2012) S29–S37.
[49] E. Querdel, M. Reinsch, L. Castro, D. Kose, A. Bahr, S. Reich, B. Geertz, B. Ulmer, M. Schulze, M.D. Lemoine, T. Krause, M. Lemme, J. Sani, A. Shibamiya, T. Studemann, M. Kohne, C.V. Bibra, N. Hornaschewitz, S. Pecha, Y. Nejahsie, I. Mannhardt, T. Christ, H. Reichenspurner, A. Hansen, N. Klymiuk, M. Krane, C. Kupatt, T. Eschenhagen, F. Weinberger, Human engineered heart tissue patches remuscularize the injured heart in a dose-dependent manner, Circulation 143 (20) (2021) 1991–2006.
[50] T. Studemann, J. Rossinger, C. Manthey, B. Geertz, R. Srikantharajah, C. von Bibra, A. Shibamiya, M. Kohne, A. Wiehler, J.S. Wiegert, T. Eschenhagen, F. Weinberger, Contractile force of transplanted cardiomyocytes actively supports heart function after injury, Circulation 146 (15) (2022) 1159–1169.
[51] S.Y. Wei, P.Y. Chen, C.C. Hsieh, Y.S. Chen, T.H. Chen, Y.S. Yu, M.C. Tsai, R.H. Xie, G.Y. Chen, G.C. Yin, J.M. Melero-Martin, Y.C. Chen, Engineering large and geometrically controlled vascularized nerve tissue in collagen hydrogels to restore large-sized volumetric muscle loss, Biomaterials 303 (2023) 122402.
[52] M.V. Plikus, X. Wang, S. Sinha, E. Forte, S.M. Thompson, E.L. Herzog, R.R. Driskell, N. Rosenthal, J. Biernaskie, V. Horsley, Fibroblasts: origins, definitions, and functions in health and disease, Cell 184 (15) (2021) 3852–3872.
[53] M. Zhang, F. Zhao, X. Zhang, L.A. Brouwer, J.K. Burgess, M.C. Harmsen, Fibroblasts alter the physical properties of dermal ECM-derived hydrogels to create a pro-angiogenic microenvironment, Mater Today Bio 23 (2023) 100842.